Order Number 1330895

The use of surface hot-film sensors in dilute polymer flows

Goforth, Montgomery Bailey, M.S.

Rice University, 1987

U·M·I
300 N. Zeeb Rd.
Ann Arbor, MI 48106

RICE UNIVERSITY

THE USE OF SURFACE HOT-FILM SENSORS IN DILUTE POLYMER FLOWS

by

MONTGOMERY BAILEY GOFORTH

A THESIS SUBMITTED
IN PARTIAL FULFILLMENT OF THE
REQUIREMENTS FOR THE DEGREE

MASTER OF SCIENCE

APPROVED, THESIS COMMITTEE:

William F. Walker, Professor
of Mechanical Engineering, Chairman

Alan J. Chapman, Professor
of Mechanical Engineering

Frederic A. Wierum, Professor
of Mechanical Engineering

Houston, Texas

November, 1986

ABSTRACT

The purpose of this study was to assess the feasibility of using flush-mounted surface hot-film sensors in dilute polymer solutions to measure mean wall shear stress. Experiments were conducted using hot-film sensors mounted on the surface of a rotating disk. It is shown that a sensor calibration obtained in a pure water flow cannot be used directly to provide accurate skin friction measurements in a dilute polymer flow. However, the repeatability of the results suggests that a functional relation may exist between a sensor's calibration in water and in dilute polymer, thereby permitting precalibration of the sensor in pure water. It is also possible that reasonably consistent measurements may be obtained by precalibration of sensors in controlled polymer solutions.

Experiments were also conducted by injecting concentrated polymer solution (4000 ppm) into the boundary layer of the rotating disk. Drag reduction and hot-film performance comparable to that obtained with homogeneous dilute polymer solution was demonstrated.

ACKNOWLEDGEMENTS

I wish to thank Dr. Michael Reischman of the Office of Naval Research, Fluid Mechanics Program for his funding of the project on which this work is based and Mr. Wayne Haigh of Sierra Engineering Associates, who was instrumental in planning the project. Thanks are also due to Dynamics Technology, Inc. and especially to Dr. Robert L. Gran and Dr. Dennis K. McLaughlin for their continued advice and support throughout the course of the project.

I would also like to thank Dr. William F. Walker, my advisor, for his constant support during my long history of graduate studies.

A heartfelt thanks is also due my typists, Marie Benoit and Linda Anderson. Their invaluable skills made the completion of this work a considerably lesser burden.

Finally, my thanks, and my love, go to my wife Alyssa, for all of her caring.

TABLE OF CONTENTS

ILLUSTRATIONS

1. INTRODUCTION

The U. S. Navy and other government agencies have shown significant interest in vehicle drag reduction over the past several decades. Much of the research in this area has concentrated on the reduction of skin friction drag which is the major drag component for a slender body. Drag reduction can enhance the design and operational flexibility of a vehicle by increasing its maximum speed, decreasing power requirements (and, hence, power plant noise), increasing range and/or payload, and decreasing acoustic and non-acoustic signatures. Of particular interest is the injection of a dilute polymer solution into the turbulent boundary layer on the vehicle, a technique which has proven to be effective in reducing skin friction drag.

Several technical issues in drag reduction in dilute polymer solution need improved understanding if this technology is to be carried through to operational application. These include the effect of dilute polymers on the turbulence structure, the mixing and dilution of the polymer in the boundary layer downstream of injection and the subsequent effect on drag reduction, and the degradation of the polymer molecules under high shear conditions. Investigation of the latter two topics would be enhanced by the measurement of local skin friction in order to determine the effects of polymer dilution and/or shear degradation. Local skin friction measurements would also be useful in model studies as a means of optimizing polymer injection techniques.

In the past, quantitative measurements of skin friction have been accomplished by measuring a pipe flow's pressure drop or by means of drag balances, Preston and Stanton tubes and laser Doppler velocimetry (LDV) to name several. However, the first two methods measure only the total skin friction drag. "Floating element" drag balances tend to be expensive and fragile. LDV techniques have insufficient resolution to probe the very thin viscous sublayer of a high-speed flow and the "tube-type" probes become fouled by polymer molecules.

One other technique that has also been used is a surface hot-film for which the heat transfer to the fluid is related to the skin friction. The use of surface hot-film sensors in pure water flows was pioneered by Liepmann and Skinner (1954) with later contributions by Bellhause and Schultz (1966) and Brown and Davey (1971). The use of a surface hot-film sensor for local skin friction measurements in other than pure water flows was recently demonstrated by Madavan, Deutsch and Merkle (1985) in experiments on drag reduction using microbubble injection.

Despite the large amount of research that has been conducted with drag reducing dilute polymers, there is apparently no reported application of surface hot-film sensors for wall shear measurements in dilute polymer flows. Kraynik and Schowalter (1981) have used a surface hot-film with apparent success in comparatively concentrated solutions of polymers. In addition, some success has been achieved with hot-film anemometers in dilute polymer flows (Kalashnikov and Kudin, 1973). However, the use of hot-film probes apparently requires frequent cleaning to remove mucus buildup and calibration shifts were

apparent in the data (Lindgren and Chao, 1967). The goal of the present project was to assess the usefulness of flush-mounted surface hot-film gages for the measurement of local skin friction in a dilute polymer flow.

The first step in the assessment was the validation of our hot-film calibration technique in pure water. The degree and type of calibration changes during a single experimental day and between days were examined. Similarly, calibration changes for flush-mounted surface hot-film sensors immersed in a dilute polymer solution were examined. The flowfield chosen for the experimental evaluation is that which accompanies an unconfined rotating disk (Figure 1). With this flowfield, high wall shear stresses, typical of a high-speed turbulent boundary layer flow, are easily obtainable. In addition, the flowfield has been analytically characterized (by von Kármán, 1921 and by Granville, 1973).

The local wall shear stress in the polymer solution was determined from the sensor output and the sensor's calibration in pure water. The local wall shear stress reduction obtained in this manner was then compared to the measured torque reduction on the rotating disk. Additional comparisons were made to experimental results of Hoyt and Fabula (1964) and the maximum drag reduction asymptote of Virk, et al. (1970) as presented by Granville (1973).

The effects of the injection of a concentrated polymer solution into the boundary layer of the rotating disk on the hot-film sensors' output and on the driving torque were also examined.

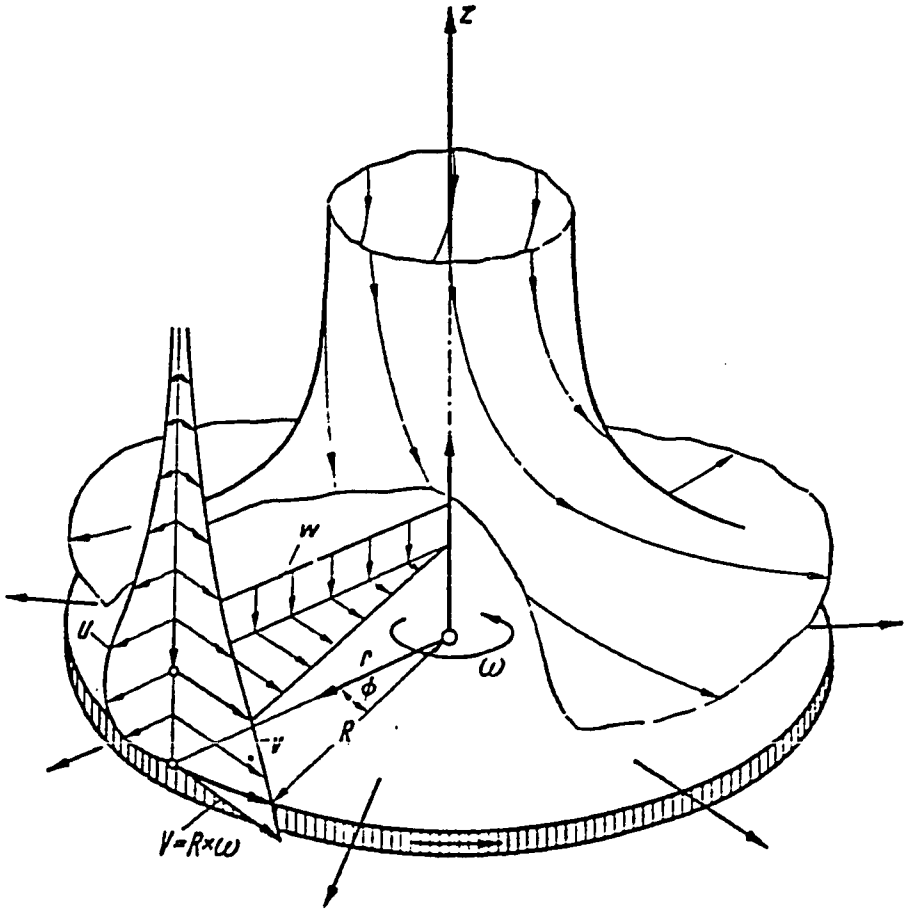

Figure 1. Idealized Flowfield for the Case of a Disk Rotating in an Infinite Fluid

The second section describes the experimental apparatus, the instrumentation and the experimental procedures. Section 3 describes the data processing methods. Section 4 presents the experimental results, first of the power measurements and second the hot-film sensor measurements with homogeneous solutions of dilute polymer. The last part of Section 4 describes the results of measurements made with injection of concentrated solutions of polymer into the central stagnation region of the rotating disk (in otherwise pure water). Finally, Section 5 presents the conclusions of the study.

2. FACILITY AND INSTRUMENTATION

2.1 Facility

In order to obtain high wall shear stresses, the flowfield chosen for the experimental evaluation is that accompanying an unconfined rotating disk. The apparatus used to approximate this flowfield consists of a rotating disk suspended in a large tank of fluid. Since the fluid is not infinite in extent, it would be expected that the angular momentum imparted by the disk on the fluid would increase with time leading to solid body rotation. This would significantly reduce the angular velocity of the disk relative to the fluid which, in turn, would reduce the observed drag on the disk.

In order to suppress the transfer of angular momentum to the fluid, baffles were placed on the sides of the test tank. However, these baffles generated large scale turbulence throughout the test tank which then affected the flowfield approaching the surface of the disk. A cylindrical shroud was positioned near the disk to compensate for this effect. The baffle and shroud arrangement was shown by dye flow visualization to produce an incoming flowfield very similar to that postulated by von Kármán (1921) and others in their theoretical analyses of this flowfield.

A schematic of the rotating disk test facility is shown in Figure 2. The 23.9 cm diameter disk is suspended 38 cm above the

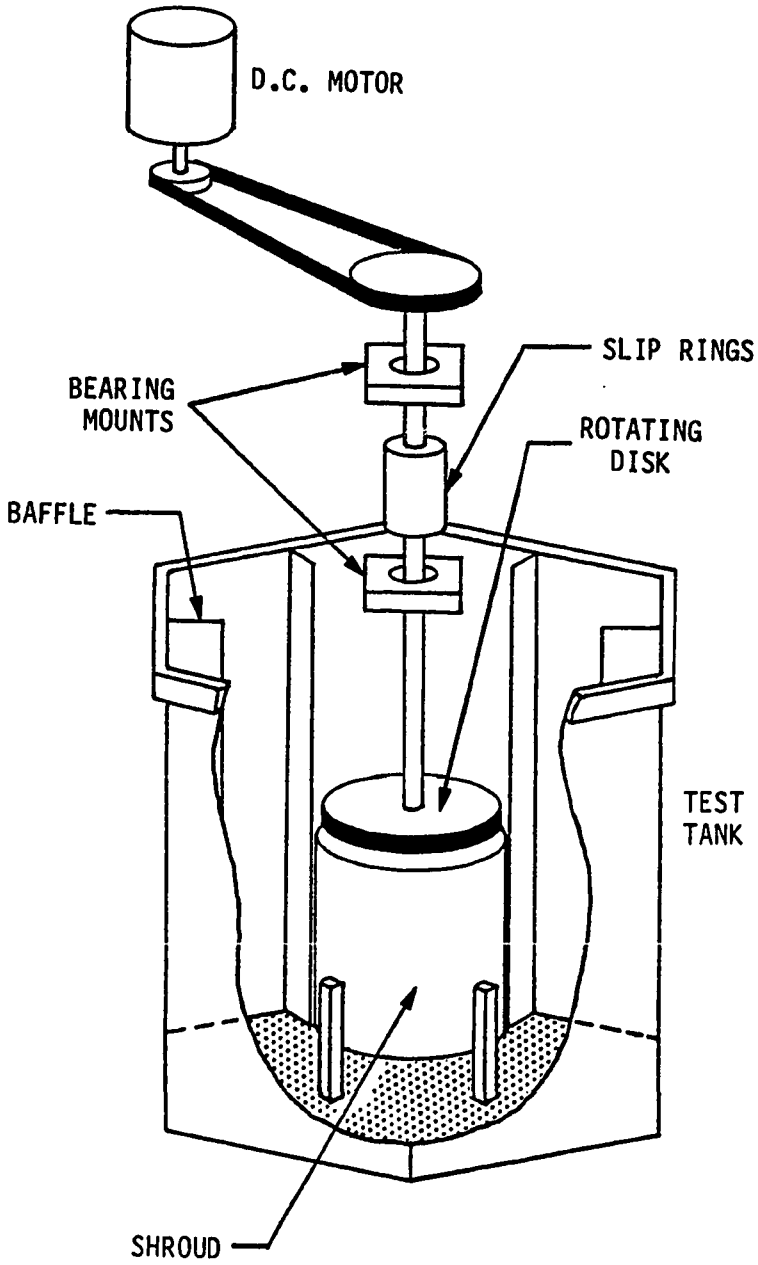

Figure 2. Schematic of Test Facility

floor of a 208 liter hexagonal tank constructed from acrylic plastic. The tank has baffles located on its sidewalls and a cylindrical shroud (24.8 cm I.D.) positioned just below the disk. In addition to the baffles and the shroud, the test tank also contains an injection tube rising vertically from the bottom of the tank toward the center of the disk (Figure 3). This tube was used to inject dye for flow visualization and to inject concentrated polymer solution as described in Section 4.3.

The disk is attached to a 2.5 cm O.D. stainless steel shaft that is driven via a belt and pulley arrangement by a 1.5 kW D.C. motor. A sectional view of the disk (made in two parts) is shown in Figure 4. The upper plate is aluminum and attaches directly to the stainless steel shaft. The lower stainless steel plate is attached to the upper plate such that a cavity roughly 0.64 cm high and 21 cm in diameter exists between the two. This cavity is made water tight by the use of an O-ring seal. Six hot-film sensor mounting locations are machined into the lower surface of the disk. These locations are placed at equally spaced radial positions ranging from r = 2.858 cm to 9.385 cm. The surface hot-film sensors, held by delrin collars, are mounted in the disk using a brass cap and O-ring assembly as shown in Figure 5. These O-rings serve both as a water tight seal and a spring to flush-mount the sensors.

2.2 Hot-Film Instrumentation

The hot-film control electronics used for the present study is a DISA, type 56C12, symmetrical bridge, constant-temperature anemometer.

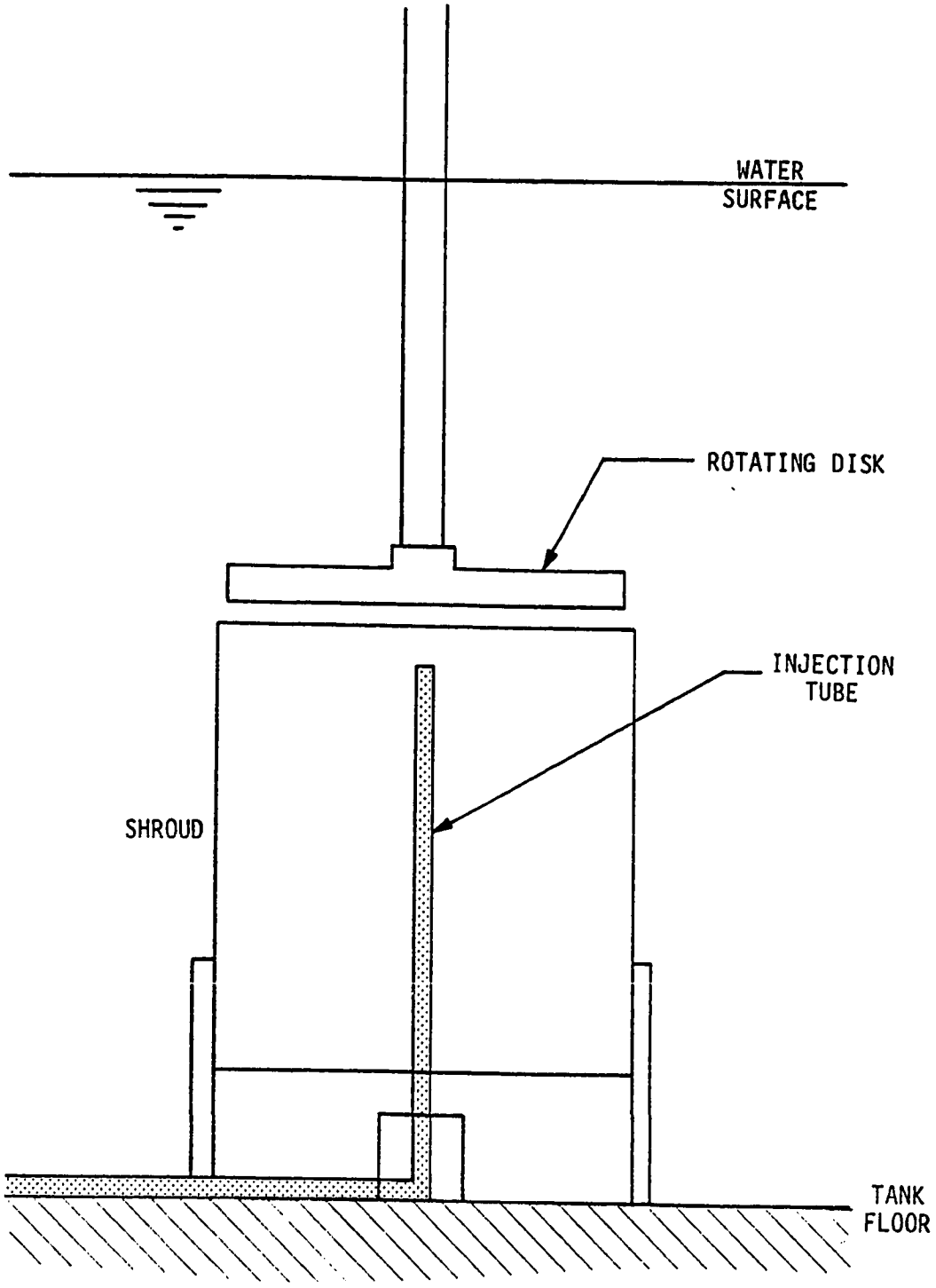

Figure 3. Schematic of the Injection System

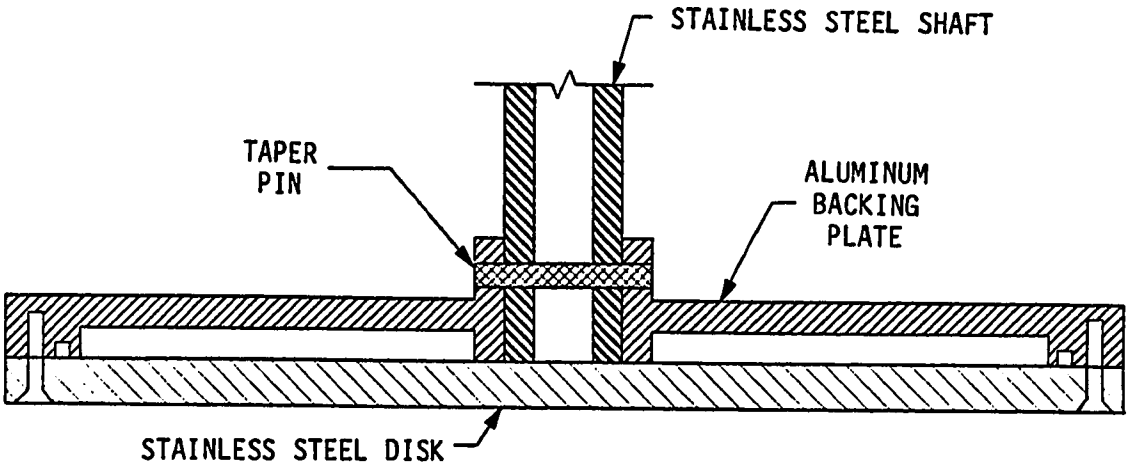

Figure 4. Sectional View of Disk

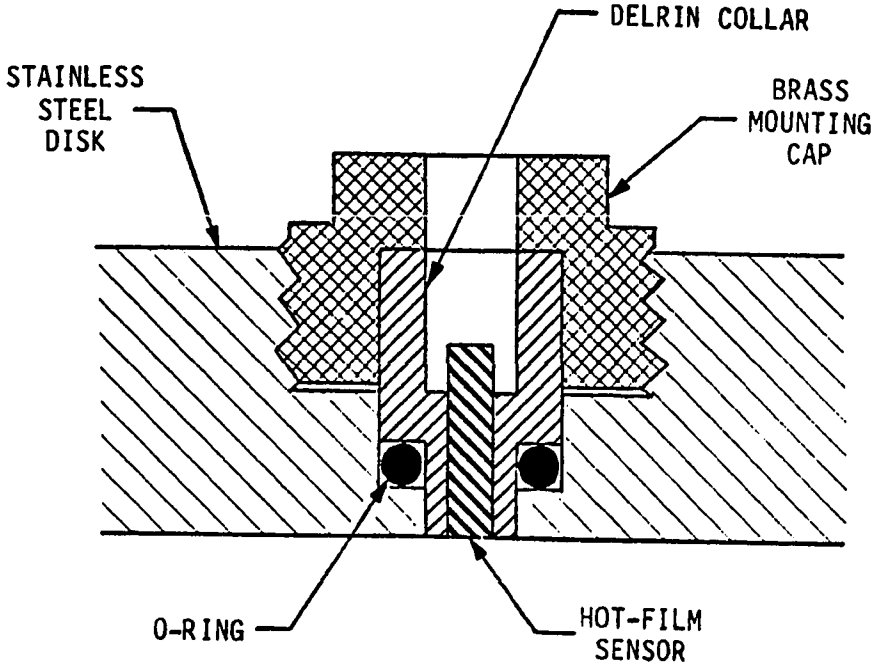

Figure 5. Close-up of Probe Mounting Location

The sensors are TSI, miniature, flush-mount, platinum hot-films (model 1268W). A sensor consists of a thin film of platinum sputtered onto the end of an alumina coated quartz rod. For water use, the platinum film is covered with a thin quartz coating to prevent short circuiting. A sketch of this sensor is shown in Figure 6. The sensors were installed in the disk as discussed in Section 2.1 and were electronically connected to the DISA anemometers through slip rings manufactured by the IEC Corporation of Austin, Texas (model IEL-HS).

2.3 Auxiliary Instrumentation

To provide an estimate of the overall torque on the rotating disk, the voltage and electrical current delivered to the motor were measured and recorded. The disk rotation rate was measured using a light source and photodiode arrangement as shown in Figure 7. The shaft was covered with two substances having different reflective properties. When the shaft rotates, the resultant variation in photodiode output determines its rotation rate in a manner described in Section 3.1.

2.4 Data Acquisition

All data were acquired with a multi-channel, 12-bit, Trans-Era MDAS-7000 data acquisition system interfaced to a Hewlett-Packard HP-9920 laboratory computer for data storage and processing. In its normal configuration, the data acquisition system obtains data from 4 or 5 input channels consisting of the photodiode, the power supply

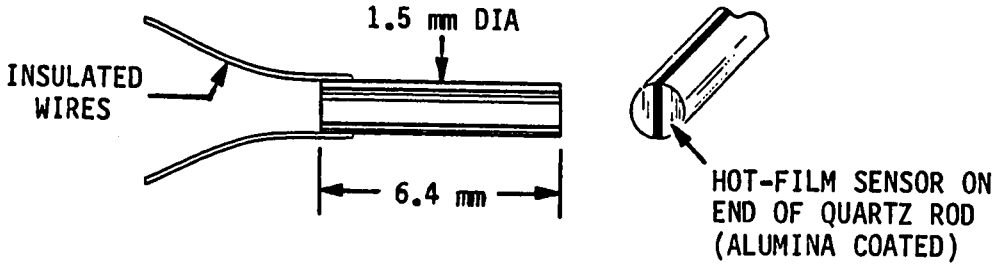

Figure 6. The Hot-Film Sensor

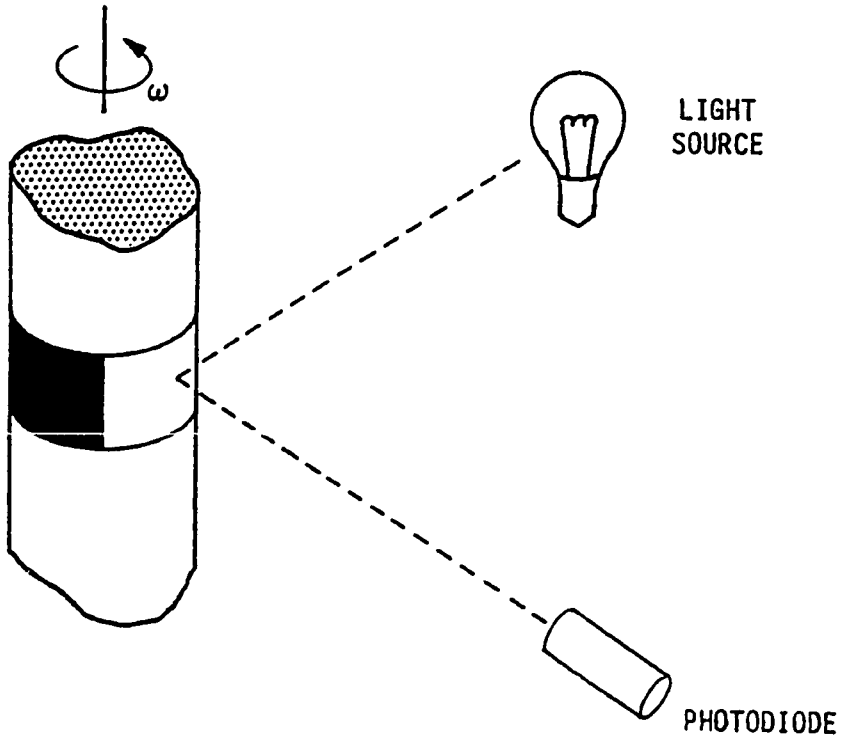

Figure 7. The Rotation Rate Sensor Apparatus

voltmeter and ammeter, and one or two of the hot-film anemometers.

During the experiments the photodiode and motor power supply signals were sampled at 1000 Hz for 1 second and the hot-film output signals were sampled at 500 Hz for 3 seconds.

2.5 Mixing Technique for Polymer Solutions

Two types of solutions were prepared for the dilute polymer experiments. The majority of experiments were conducted with the tank filled with a homogeneous solution of 100 ppm SEPARAN AP-30; these are called "polymer-ocean" experiments. For a limited number of experiments, called "injection" experiments, 4000 ppm (SEPARAN AP-30) solution was injected toward the disk in a tank of pure water as indicated by the sketch in Figure 3. Both solutions were initially prepared in a manner similar to that described by Tiederman, Luchik and Bogard (1985). Separate crystals of polymer were sprinkled into stirred water that had previously been de-aerated by boiling. The 4000 ppm mixtures were allowed to stand for about 12 hours with intermittent stirring to insure the solution was well hydrated.

For the polymer injection experiments, dye was added to the 4000 ppm solution for flow visualization. The polymer solution was gravity fed to the injection tube (Figure 3). For the polymer-ocean experiments, the 4000 ppm solution was diluted to 100 ppm in a separate 300 gallon tank and allowed to sit for an additional 12 hours with occasional stirring.

3. DATA PROCESSING

3.1 Photodiode RPM Counter

A sample of the photodiode output signal is shown in Figure 8. The output voltage was approximately -0.32 volts when the light source was reflecting off the darkened half of the rotating shaft and -0.43 volts when the light source was reflecting off the silvered portion (see Figure 7). This output was converted into the disk rotation frequency using a digital counter. A threshold level was set at a level between the maximum and minimum values of the stored photodiode signal. The number of below-to-above crossings of the threshold was then counted and the time between the first and last of these crossings was determined.

3.2 Power Supply

The voltage and current delivered by the power supply to the D.C. motor were measured both by meters on the power supply and by the data acquisition system. Current was determined by measuring the voltage drop across a high power, precision series resistor. The meters on the power supply provide time averaged measures of the output voltage and current, while the data acquisition system samples a 1 second long record of instantaneous values. The average power output during a typical sample is computed from the time averages of the voltage and current:

$$P_I = \bar{E}\,\bar{I}.$$

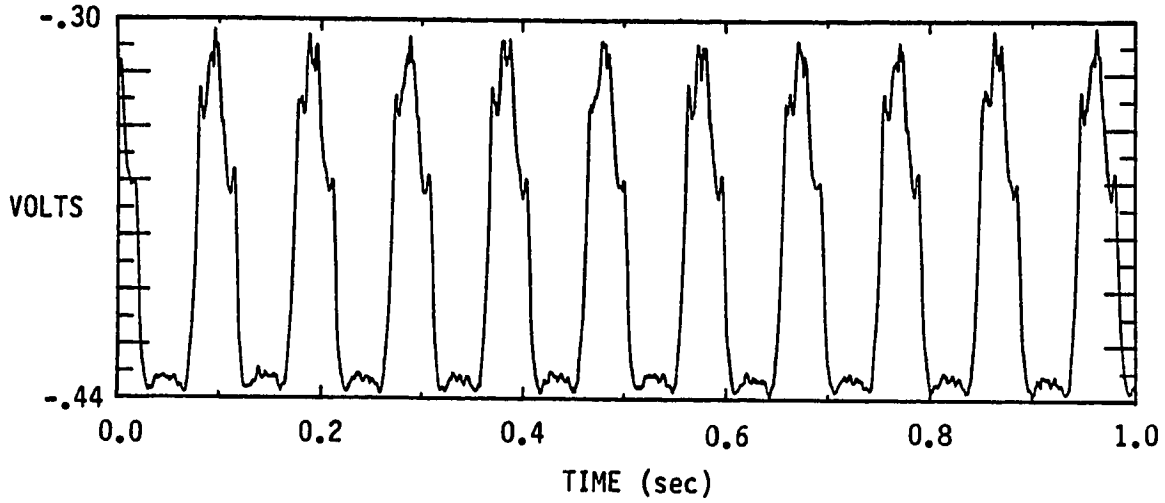

Figure 8. Rotation Rate Sensor Output for a Typical One Second Sample at 1000 Hz

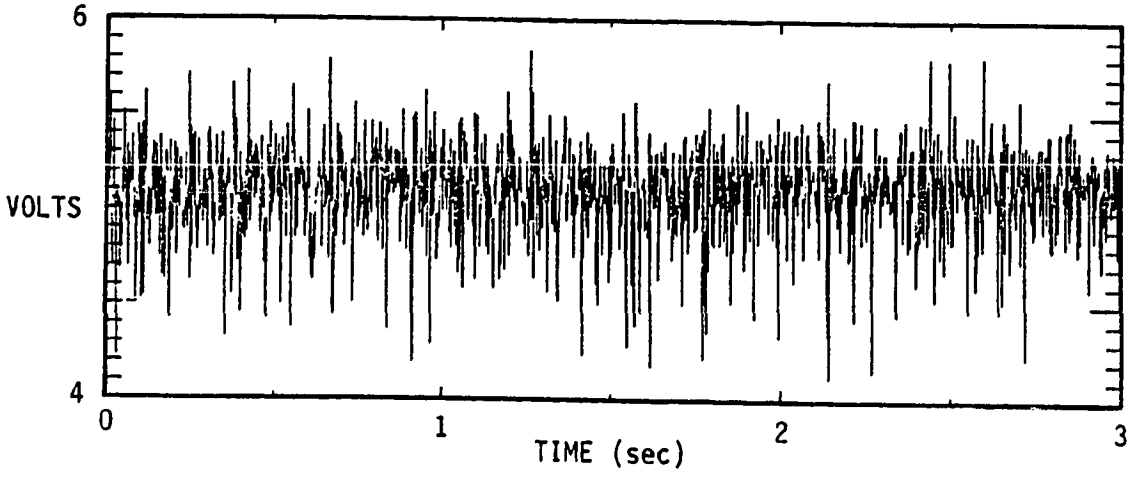

Figure 9. Hot Film Bridge Voltage Output for a Typical Three Second Sample at 500 Hz

3.3 Hot-Film Sensor Processing

A sample of the unprocessed output of a hot-film bridge circuit is shown in Figure 9. The average bridge voltage is calculated by numerically averaging these samples. The standard deviation of this signal is also determined during processing.

A heat balance for the hot-film sensor takes the form

$$\frac{E_S^2}{R_F} = (C_1 + C_2)\,\Delta T \qquad (3.1)$$

where

E_S^2/R_F is the Joule (I^2R) heating within the hot-film and ΔT is the temperature difference between the hot-film and the surrounding fluid, known as the hot-film's overheat; $C_1\,\Delta T$ represents the convective heat transfer while $C_2\,\Delta T$ represents the (approximately constant) conductive heat transfer from the hot-film to its substrate. The operating principle of the hot-film lies in the convective heat transfer coefficient, C_1, which was shown by Liepmann and Skinner (1954) to be proportional to the wall shear stress, τ_W, to the 1/3 power. Using this relationship, and the proportionality of hot-film voltage to the bridge output voltage E_B, Equation 3.1 can be written as:

$$\frac{E_B^2}{R_F \Delta T} = A\tau_W^{1/3} + B \qquad (3.2)$$

The quantity on the left hand side of the equation is the bridge power per °C of overheat. The constants A and B depend on the specific sensor and how it is mounted and therefore are obtained by calibration. This calibration involves changing the (known) wall shear stress (say, by changing the disk rotational speed) and recording the bridge voltage at a fixed overheat. Such calibrations will be given in the next section where the rotating disk shear stress is computed using analytical curve fits given by Granville for a pure liquid (no polymer additive).

Before describing the experimental results it is useful to mention that the $\tau_W^{1/3}$ scaling of the convective heat transfer coefficient results from assuming a linearly varying velocity profile and non-turbulent flow. For this situation, the theory has been experimentally verified many times. The use of this theory for a turbulent boundary layer presumes that the thermal boundary layer created by the hot-film is thinner than the viscous sublayer thickness. This requirement, in turn, places a limit on the length of the film since the thermal boundary layer thickness increases like the 1/3 power of the film length. This restriction can be written

$$(\delta_T)_{MAX} \leq \delta_V \tag{3.3}$$

where δ_V is the viscous sublayer thickness and δ_T is the thermal boundary layer thickness.

Since the turbulent boundary layer thickness can be approximated

by

$$\delta_V = 10 \frac{\nu}{U_\tau} \tag{3.4}$$

and the thermal boundary layer thickness is given by

$$\delta_T = \left[\frac{18x}{Pr(U_\tau / \nu)^2}\right]^{1/3} \tag{3.5}$$

where Pr is the Prandtl number and x is the downstream distance from the leading edge of the hot-film Equation 3.3 can be expressed as

$$\frac{L\, U_\tau}{\nu} < 55.6\ Pr \tag{3.6}$$

where L is the lenyth of the hot-film in the direction of fluid flow. For water, this relationship can be expressed as

$$L \leq 444 \frac{\nu}{U_\tau} \tag{3.7}$$

It has been verified that this restriction is satisfied in the present experiments.

4. EXPERIMENTAL RESULTS

4.1 Measurements of Power to Disk

Water Experiments

Before discussing the hot-film sensor measurements it is instructive to first present the results of the power and torque measurements under the various operating conditions. In this manner, the ability of the polymer additives to produce skin friction reduction, along with our experimental procedures, can be verified.

Figure 10 presents the motor input power $P_{I,W}$ as a function of disk rotation rate F (in RPM) for the disk fully submerged in water. The data included in this figure were obtained from 8 separate experiments conducted on two different days. For each day, the data has been grouped into that taken before the immersion of the disk into a dilute polymer solution and that taken when the disk was reimmersed in pure water after its immersion in polymer. Since there is no significant difference between the groups of data it can be concluded that the data is highly repeatable and the prior immersion of the disk in a polymer solution produces no residual effects. By a least squares curve fit, the data can be represented by:

$$P_{I,W} = 0.139\ F^{1.13}\ \text{(watts)} \qquad (4.1)$$

with a standard deviation of 4.6% about the fitted curve.

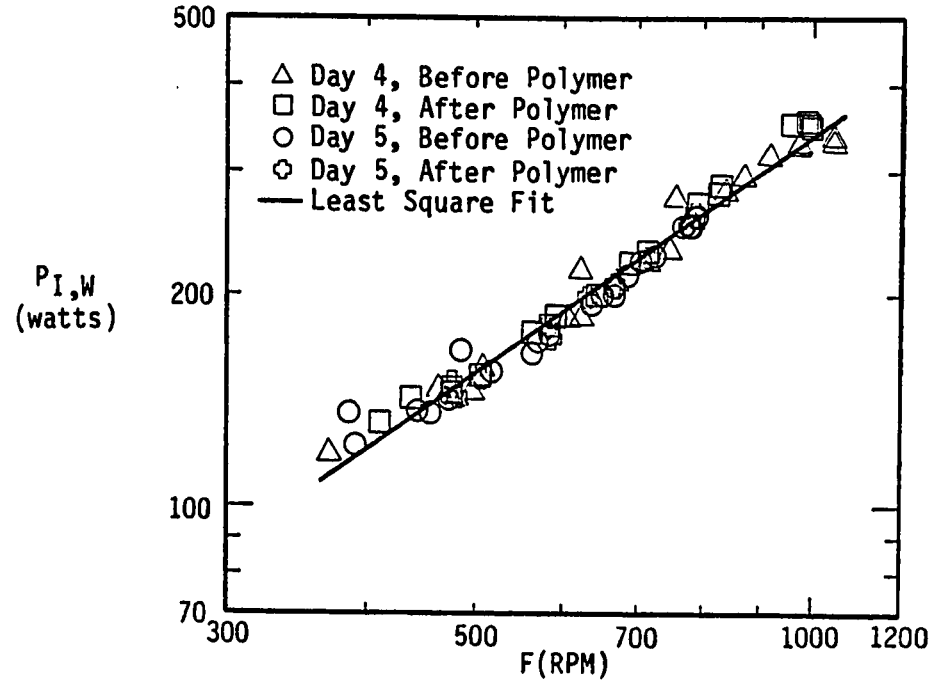

Figure 10. Motor Input Power for Rotating Disk in Water as a Function of RPM

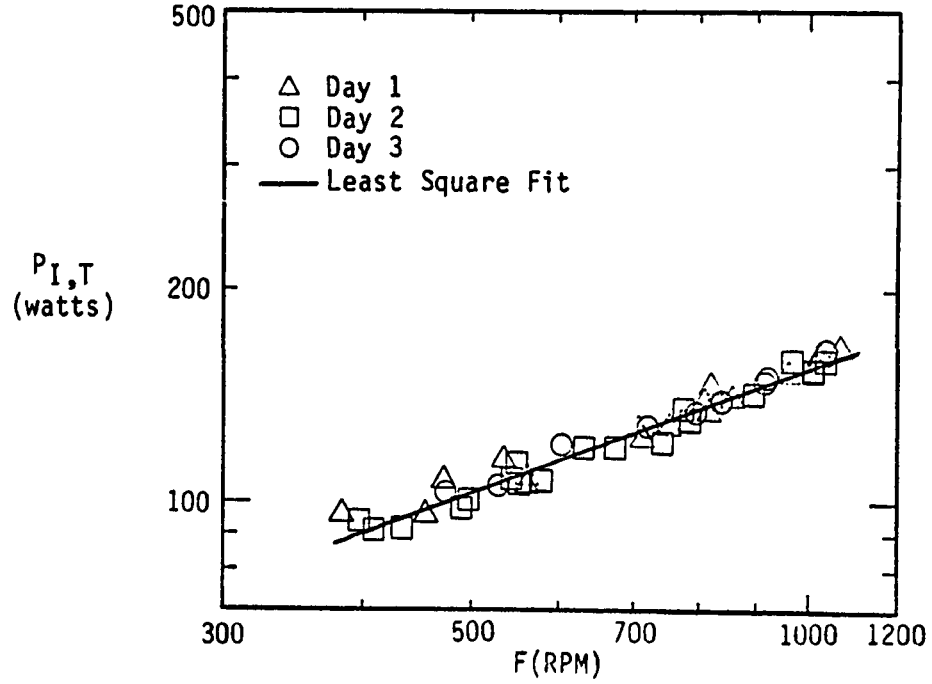

Figure 11. Motor Input Power for Rotating Disk in Air as a Function of RPM

The output power of the motor $P_o = \eta P_{I,W}$ and the motor efficiency vary considerably over the speed range. In addition, the drive pulleys, support bearings and slip rings all have resistive torques (and power dissipation) which are referred to as tare. In order to make a determination of fluid torque on the disk it is necessary to first evaluate both the motor efficiency and the tare.

Tare power was determined by operating the disk in air. Figure 11 shows the motor input power $P_{I,T}$ (tare) as a function of disk speed for rotation in air. The data were obtained in 5 separate experiments conducted on 3 different days and are grouped by days. The least squares fit to the data produces the relationship:

$$P_{I,T} = 2.51\ F^{0.597}\ \text{(watts)} \qquad (4.2)$$

with a standard deviation of 3.5% about the fitted curve.

Following the determination of tare, the motor efficiency was determined by direct measurement of the torque on the spinning disk with a hydrodynamic prony brake arrangement (shown schematically in Figure 12). The prony brake consists of a small tank of water (or glycerine/water mixture) mounted on a rolling bearing table with a calibrated spring scale on a moment arm. The tank had a set of baffles to suppress solid body fluid rotation and the disk rotation rate was controlled by the D.C. power supply output. Experiments were performed with pure water and with a glycerine/water mixture that has a 50% higher torque requirement at a given RPM.

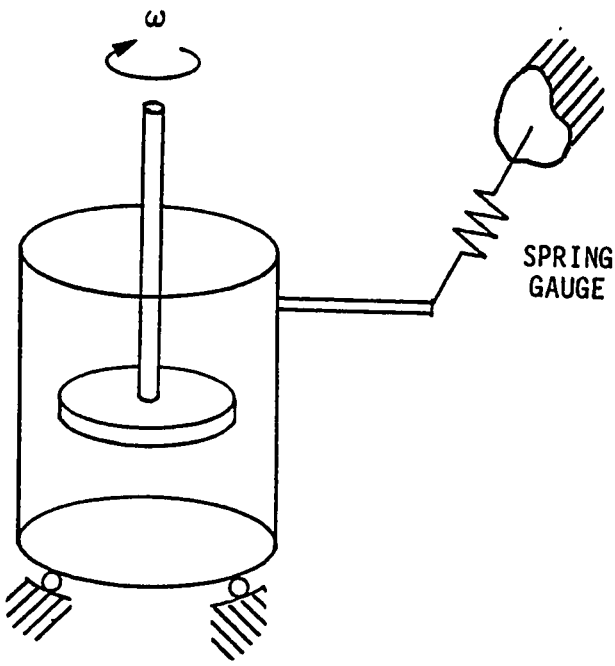

Figure 12. Schematic of the Hydrodynamic Prony Brake

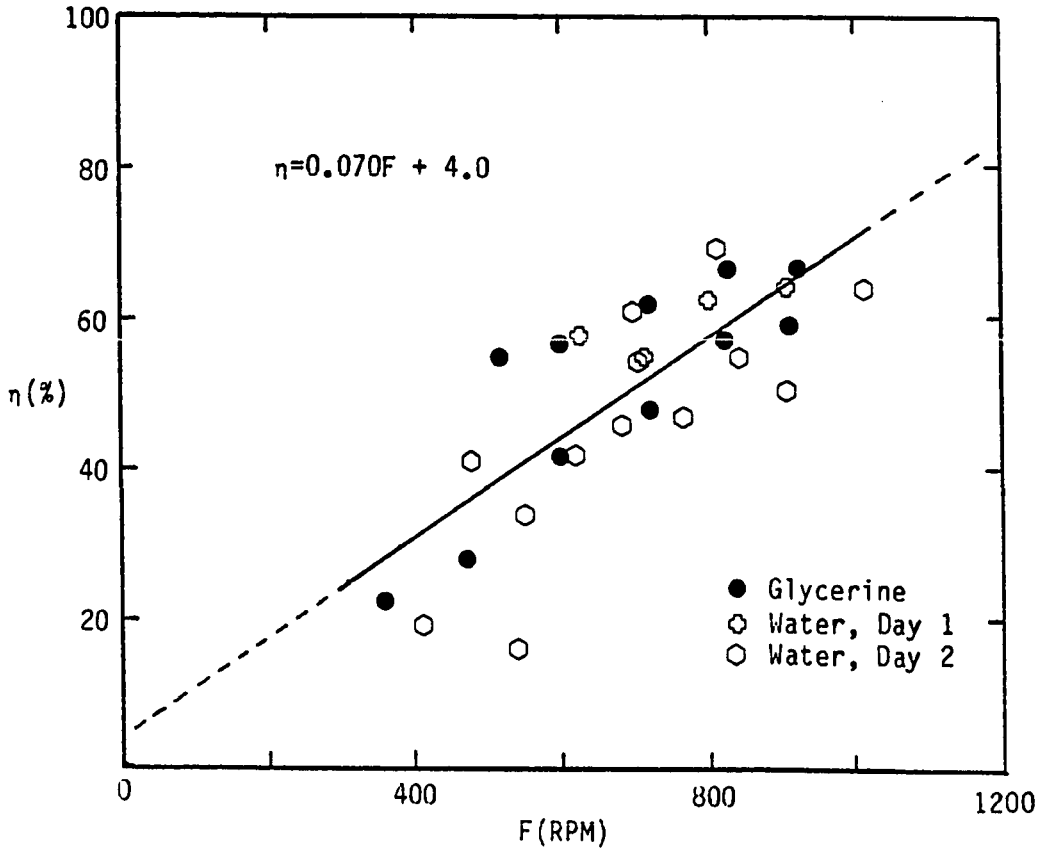

Figure 13. Motor Efficiency as a Function of Disk Rotation Rate

The results of the efficiency calibrations are plotted in Figure 13 from which a least squares fit to the data gives

$$\eta = 0.070\ F + 4\ \% \quad (400\ \text{RPM} < F < 1000\ \text{RPM}) \tag{4.3}$$

This efficiency can be used with the measured power delivered to the motor (minus tare) to determine power delivered to the disk.

$$P_{D,W} = \eta(P_{I,W} - P_{I,T}) \tag{4.4}$$

Torque T can be determined from this power and nondimensionalized to a moment coefficient with:

$$C_{M,W} = \frac{T}{\frac{1}{2}\rho\omega^2 R^5} \tag{4.5}$$

The measured power data from Figures 10 and 11 were reduced in this manner to produce the moment coefficient data shown in Figure 14. Shown also on Figure 14 is the correlation established by von Kármán, $C_{M,K} = 0.146\ Re^{-1/5}$ which is compared to the experimental results of Schmidt (1921) and Kempf (1922) in Schlicting (1979). It can be seen that the present results are roughly 10 percent higher than von Kármán's correlation. This discrepancy can be accounted for by the surface roughness of the disk and by errors in the motor efficiency calibration procedure.

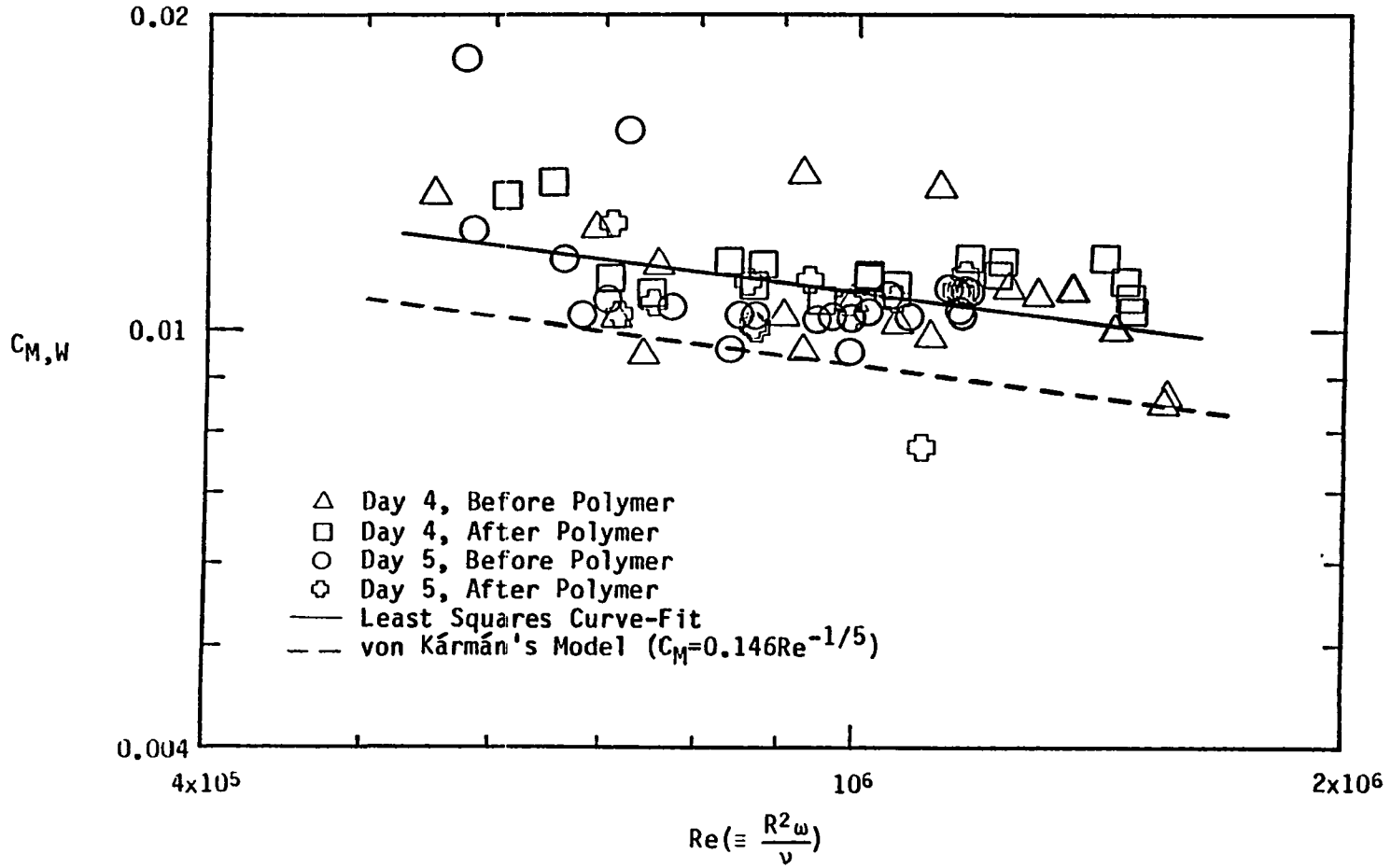

Figure 14. Measured Moment Coefficients in Water Compared to von Kármán's Model

Polymer Experiments

The power consumption measurements with a 100 ppm SEPARAN AP-30 polymer solution are plotted in Figure 15. It is evident that the power required to drive the disk is substantially less in the polymer solution than in pure water. As in the water and air measurements, the data plotted were obtained from several different experiments on 2 different days.

The actual power dissipated by the fluid can be determined for the polymer run data by using the motor efficiency and drive train tare determined from the water and air measurements. It is referred to as:

$$P_{D,P} = \eta\,(P_{I,P} - P_{I,T}), \tag{4.6}$$

and the corresponding moment coefficient $C_{M,P}$ is calculated from this power using Equation (4.4). Figure 16 shows the experimentally determined polymer solution moment coefficient $C_{M,P}$ in comparison with the water moment coefficients $C_{M,K}$ and $C_{M,W}$. These data can also be presented as percent drag reduction using:

$$\%\ DR = \frac{C_{M,W} - C_{M,P}}{C_{M,W}} \times 100 \tag{4.7}$$

which is plotted in Figure 17. Drag reductions from 30% to 45% are observed, which are in good agreement with the results obtained by Hoyt and Fabula (1964) on similar experiments with a spinning disk in

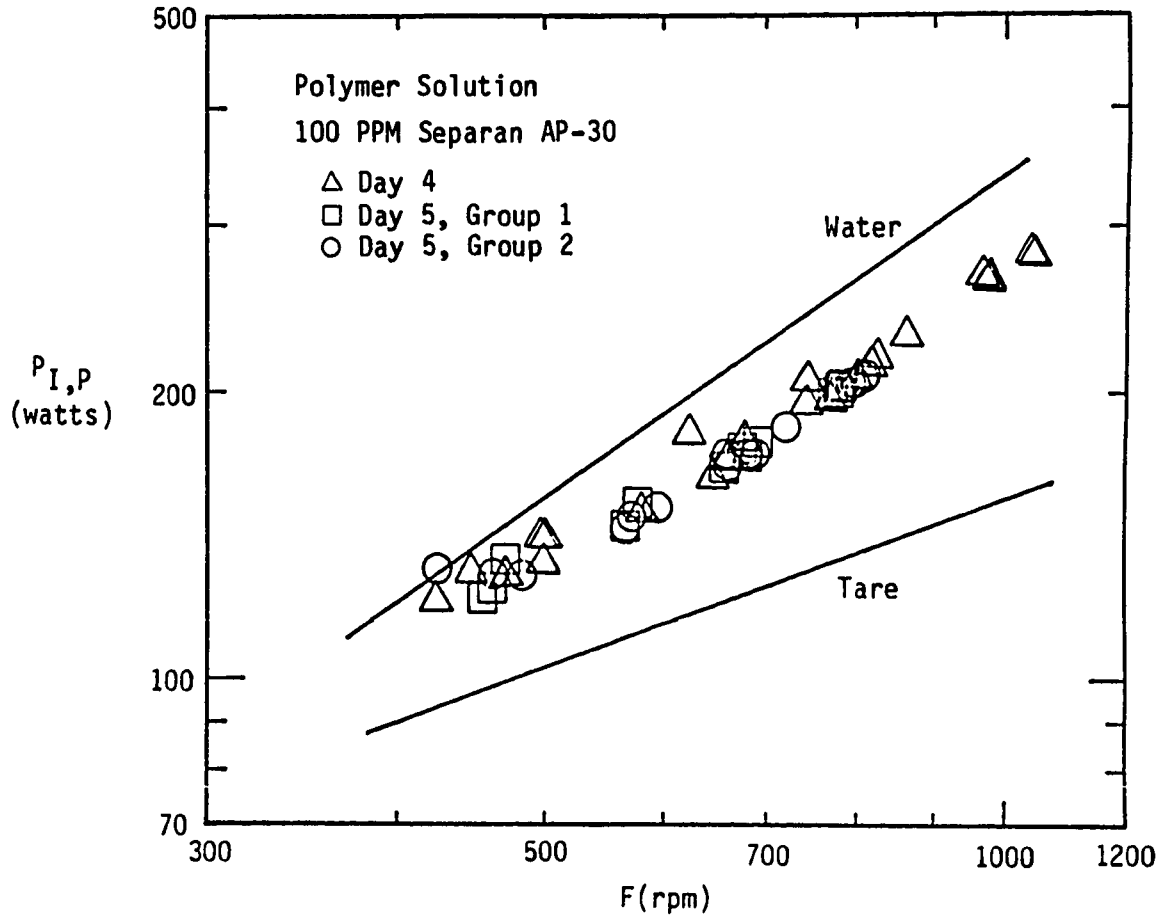

Figure 15. Motor Input Power for Rotating Disk in Polymer Solution (Curve Fits for Water and Air Runs Are Shown for Comparison

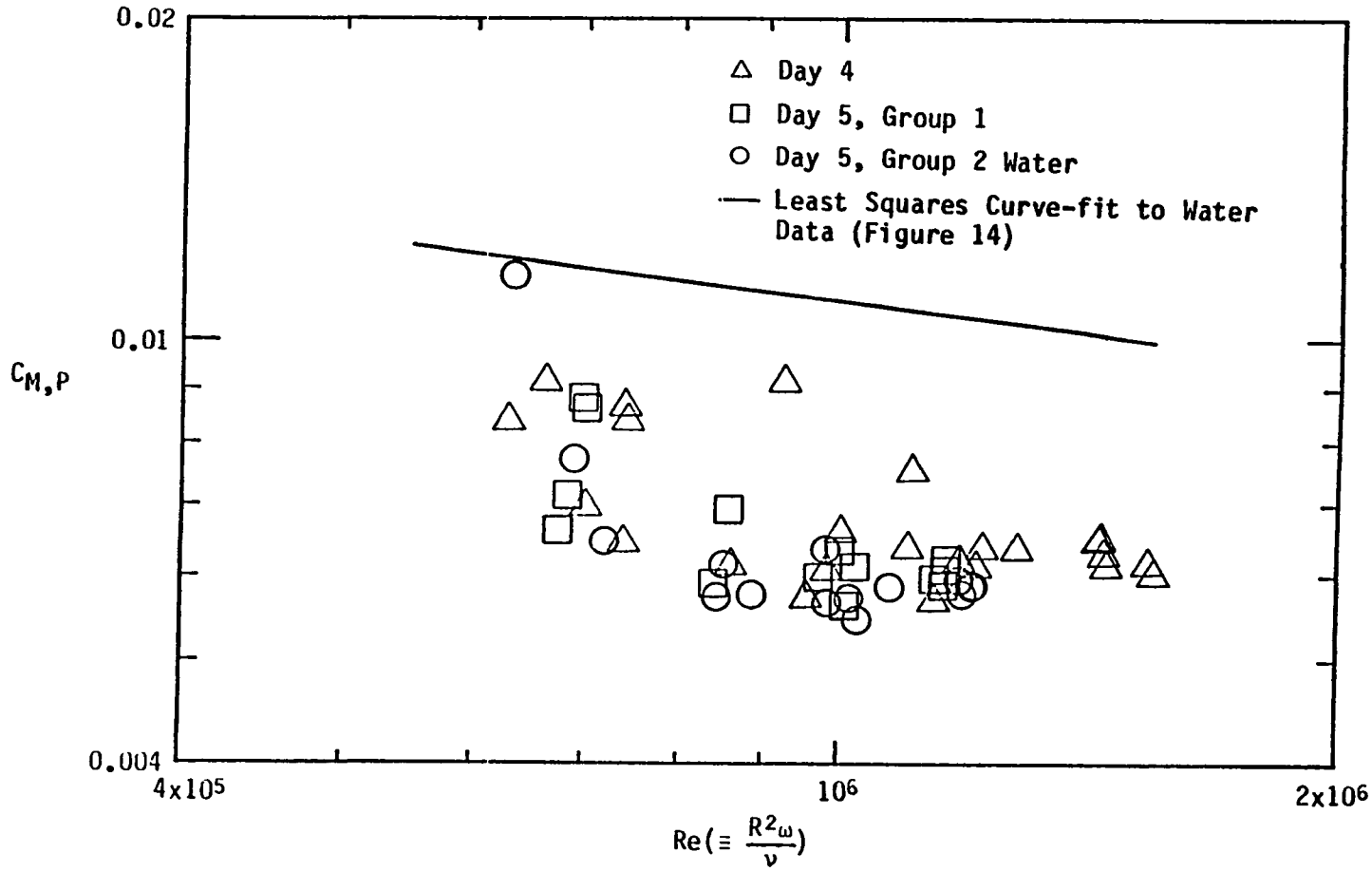

Figure 16. Measured Moment Coefficients in Dilute Polymer Solution Compared to Values Measured in Water

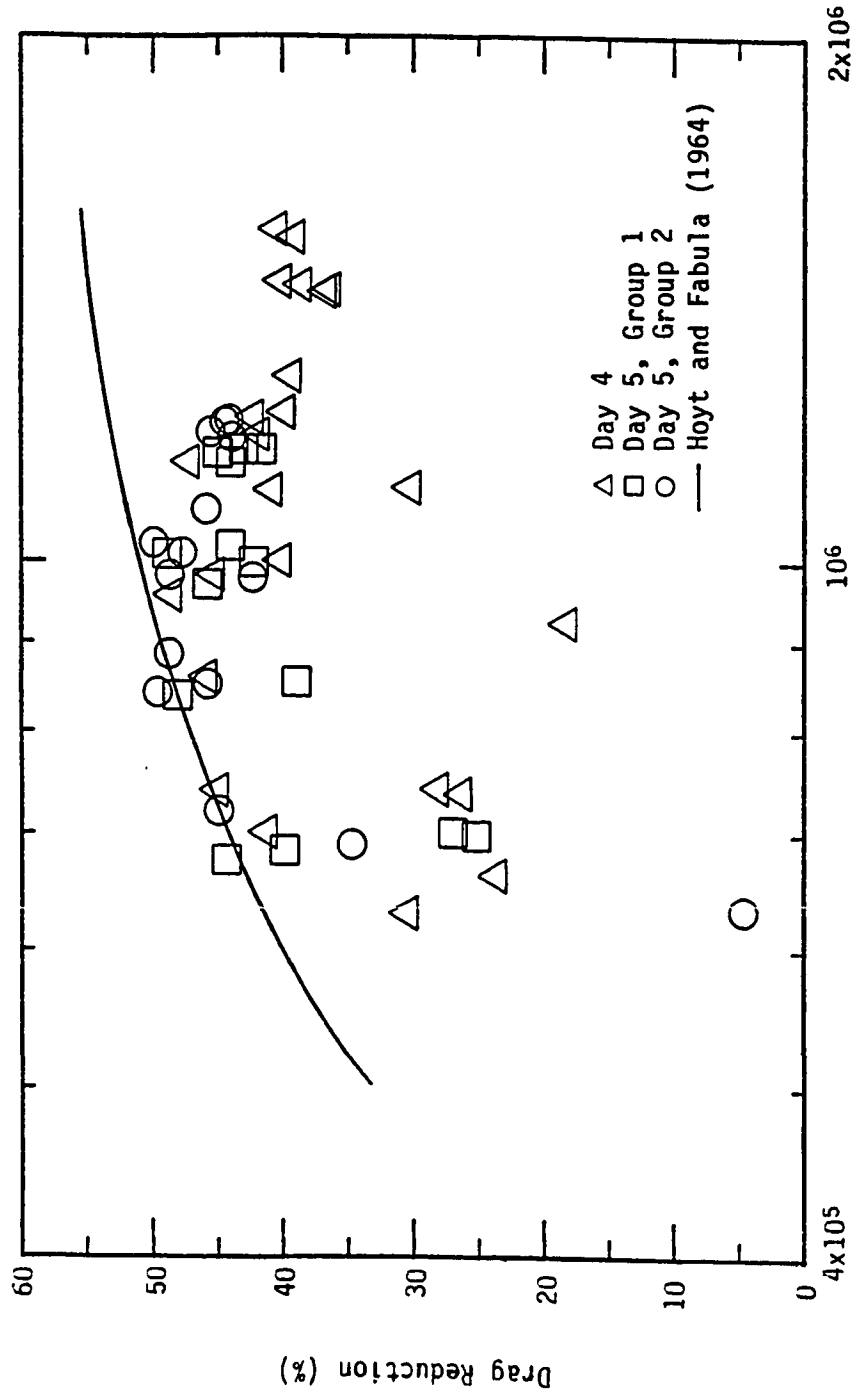

Figure 17. Percent Drag Reduction Inferred by Power Measurements

water and dilute polymer solutions. The scatter of the present %DR measurements is most likely due to inaccuracies in the power measurement which is more crude than a direct torque measurement. The present results do indicate that the spinning disk facility does operate in a manner consistent with other such facilities both with and without polymer addition.

4.2 Hot-Film Sensor Measurements

An output of one of the hot-film sensors immersed in pure water is shown in Figure 18 where the bridge power per °C of overheat (proportional to the heat flux to the water from the hot-film sensor) is plotted as a function of disk rotation rate. The data were recorded from several experiments conducted on two different days. Such results were typical of experiments on several sensors. However, it should be noted that occasional measurements would show very spurious behavior that is suspected to be caused by variations in the slip ring contact resistance. In addition, sensor output variations also resulted from mechanical failure of the electrical contacts to the sensor caused during installation of the probes in the disk.

Individual hot-film sensors are calibrated by plotting the sensor output as above as a function of wall shear stress (expressed in terms of local wall shear velocity $U_\tau = \sqrt{\tau_w/\rho}$). The wall shear velocity in water is determined from the analytical model of Granville (1973):

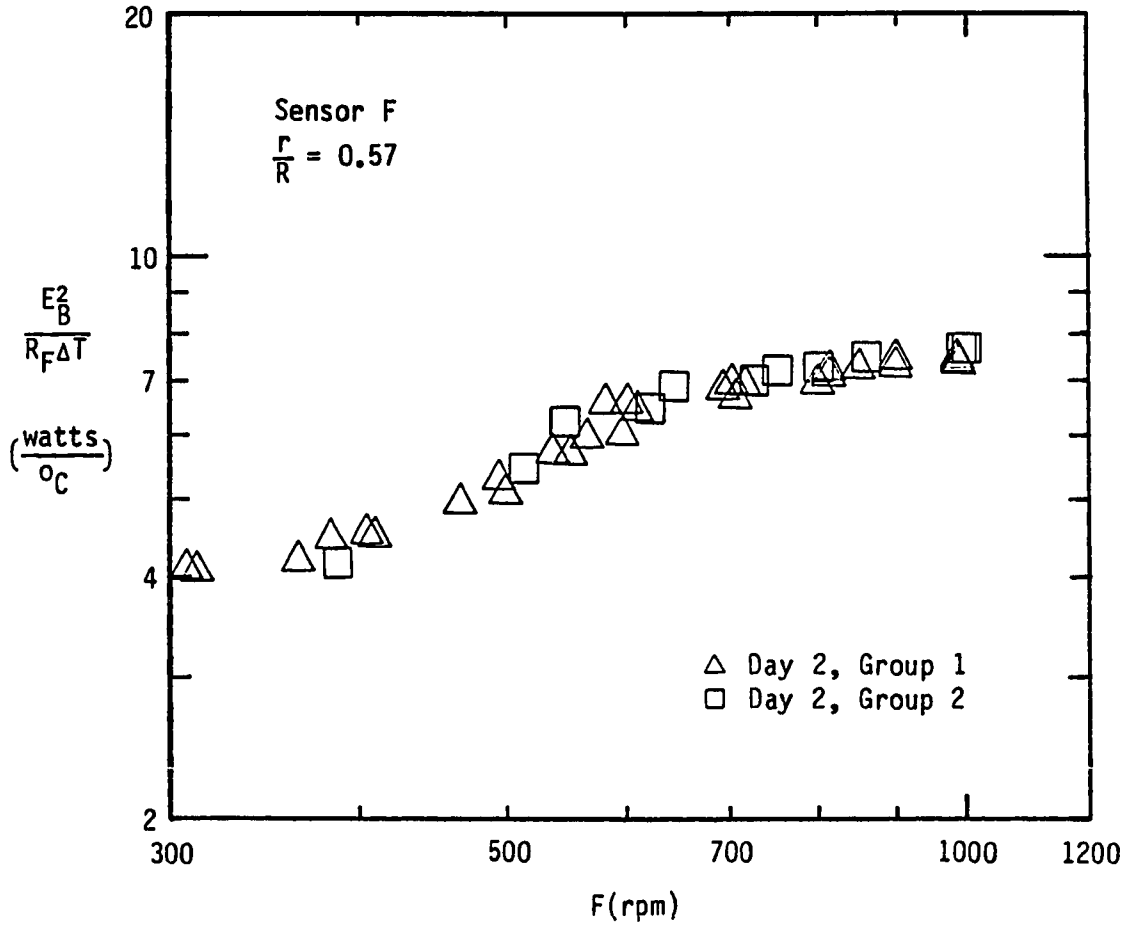

Figure 18. Hot-film Calibration Curve, Bridge Power per °C of Overheat vs. Disk Rotation Rate, for Sensor F Located at (r/R) = 0.57 on Day 2.

$$U_{\tau,w}(r,\omega) = \frac{\omega r}{4.96 \log_{10}\left(\frac{\omega r^2}{\nu}\right) - 5.74} \tag{4.8}$$

This model has been verified by comparison with velocity profiles measured by Cham and Head (1969) as well as moment coefficient data (integrated shear stress) from a number of sources.

Figure 19 shows two calibration curves for the same probe in water on separate days. A least squares curve fit is also shown in each figure, where the fit is of the form

$$\frac{E_B^2}{R_F \Delta T} = A\, U_\tau^{2/3} + B \tag{4.9}$$

as described in Section 3.3 with the change in parameters from τ_w to U_τ.

The data are within ±10% of their respective curve fits and the two curve fits differ only by the zero shift. These two figures show that a hot-film calibration curve determined in water is typically very stable throughout a measurement day and that calibration curves vary slightly when compared on a day to day basis. Similar calibration curves (on multiple experimental days) were obtained for sensors E and G. The other sensors experienced problems either with mechanical failure of sensor leads or with especially noisy slip rings (the latter is suspected). Unfortunately, no more than two sensors operated satisfactorily during any single experiment.

Figures 20 and 21 show the heat transfer measurements for two

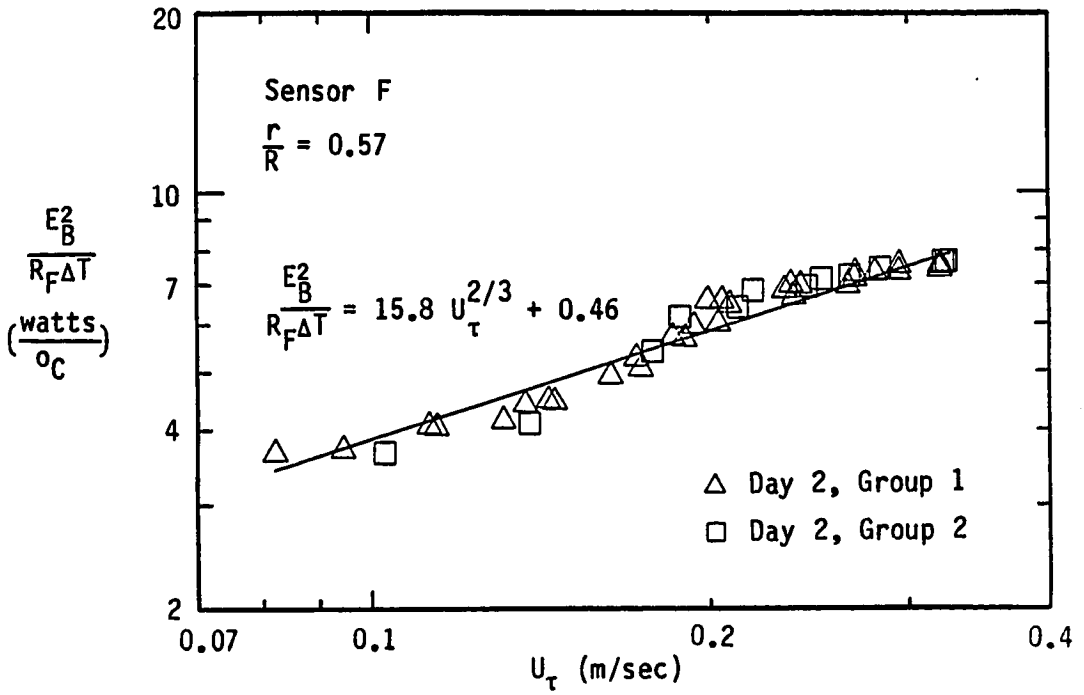

a) Day 2

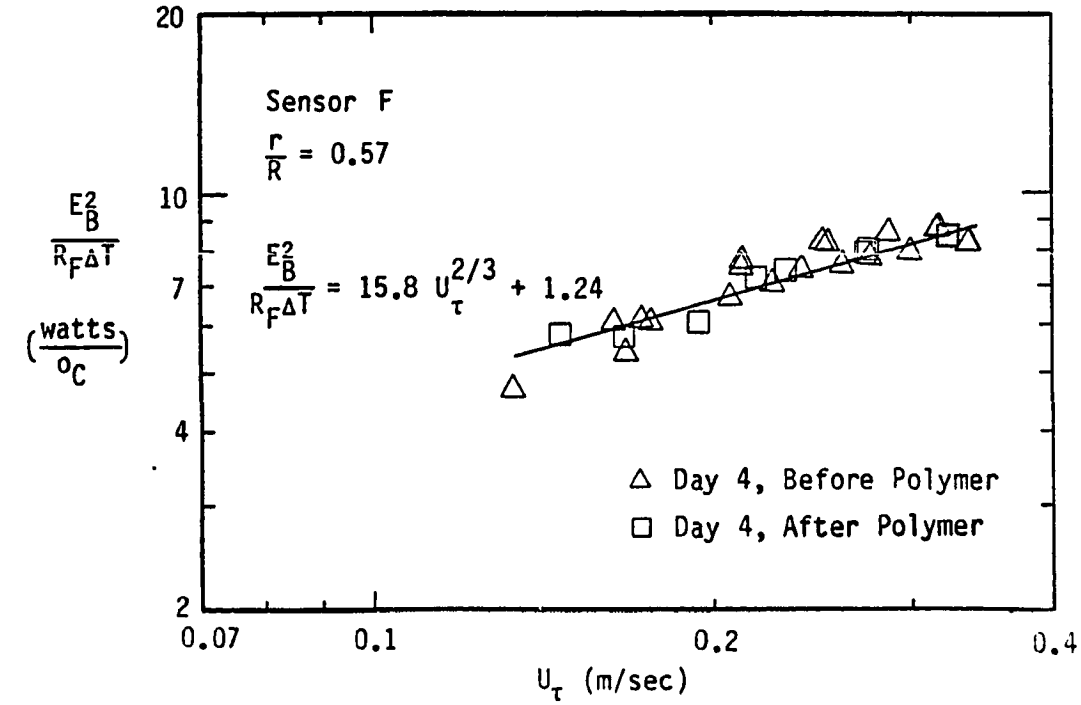

b) Day 4

Figure 19. Hot-film Calibration Curve, Bridge Power per °C of Overheat vs. U_τ, for Sensor F Located at (r/R) = 0.57 on Two Separate Days.

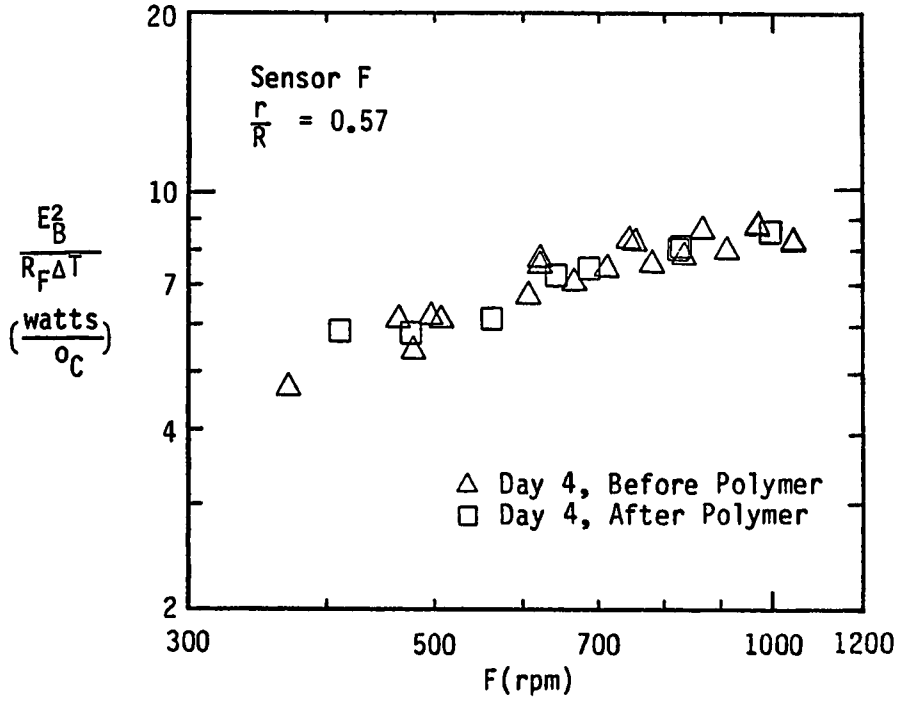

a) Immersed in Water

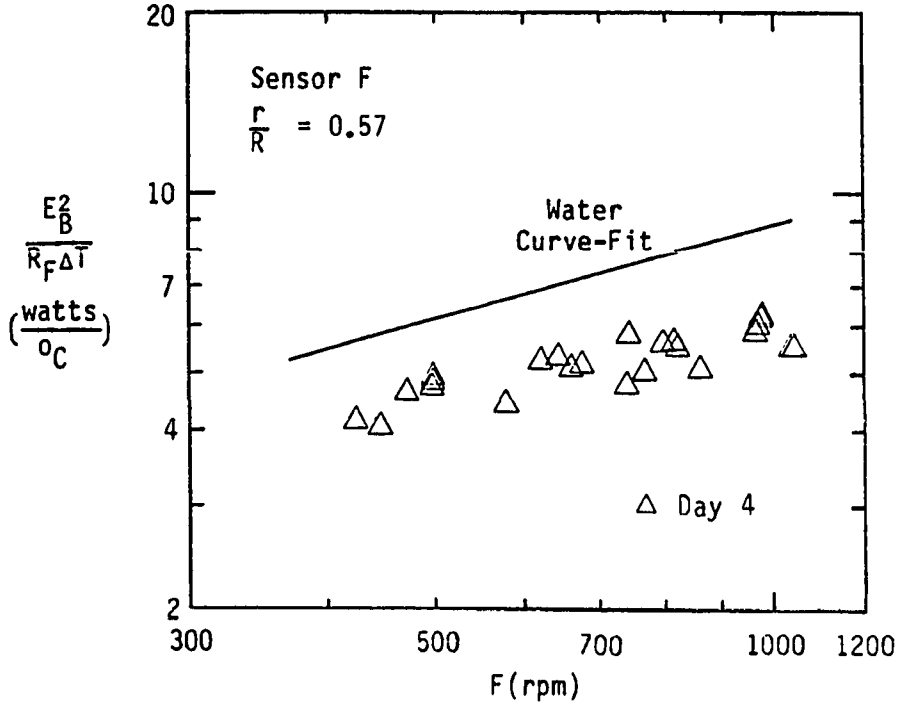

b) Immersed in a Solution of 100 PPM Separan AP-30

Figure 20. Bridge Power per °C of Overheat vs. Disk Rotation Rate, for Sensor F Located at (r/R) = 0.57, Immersed in Water and Polymer

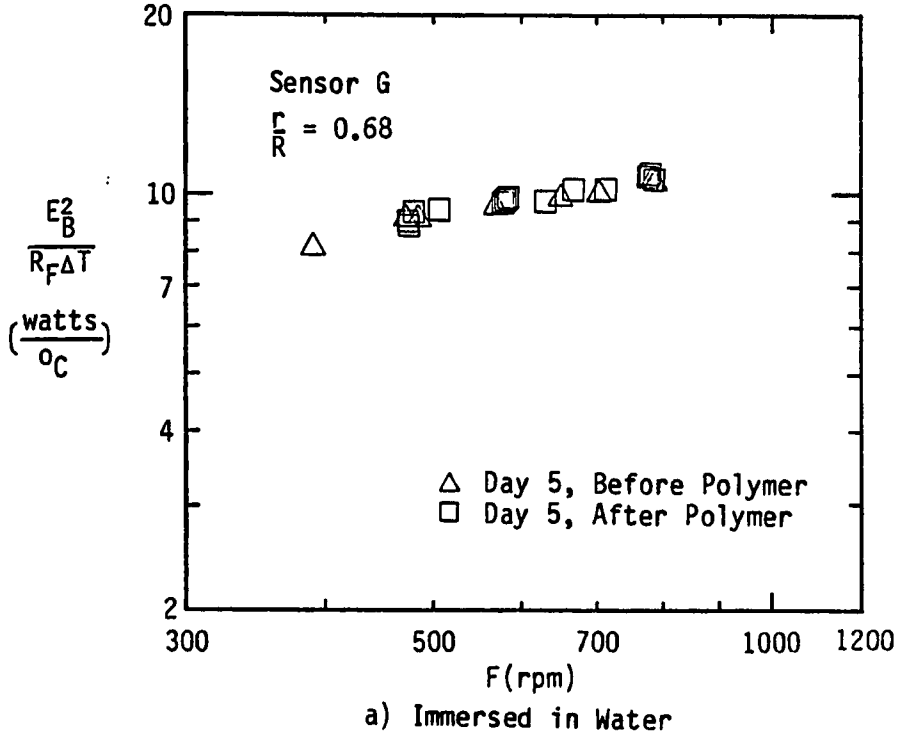

a) Immersed in Water

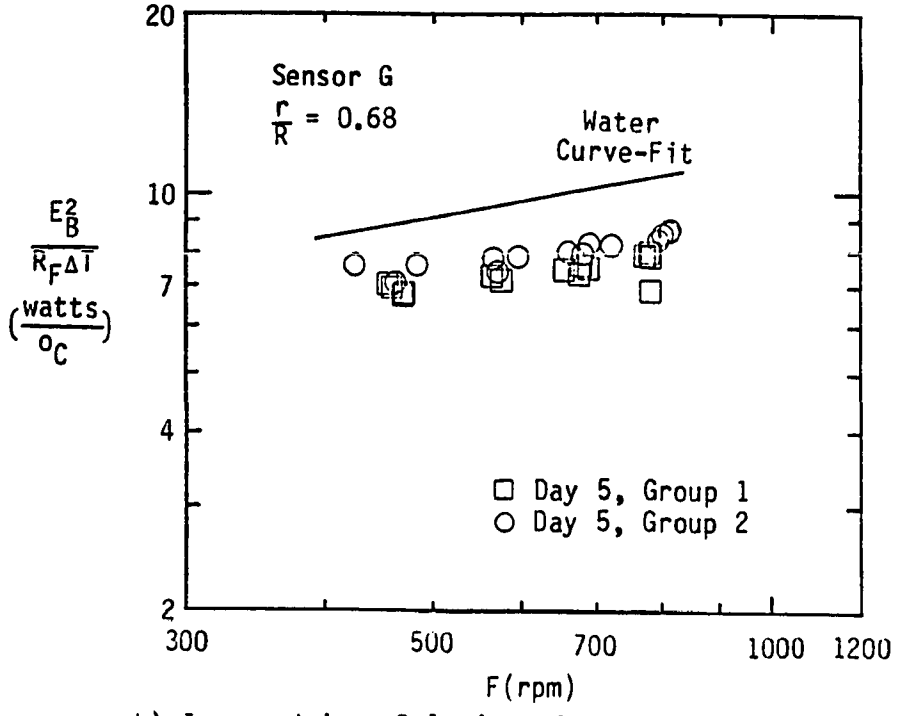

b) Immersed in a Solution of 100 PPM Separan AP-30

Figure 21. Bridge Power per °C of Overheat vs. Disk Rotation Rate, for Sensor G Located at (r/R) = 0.68, Immersed in Water and Polymer

different hot-film sensors, in water and in a 100 ppm solution of SEPARAN AP-30. The data recorded in water were taken both before and after the probes were used in the polymer solution experiments. From the relative constancy of the sensor output over the course of several individual experiments in polymer, it was established that the behavior of a flush mounted hot-film sensor immersed in a dilute polymer solution is qualitatively similar to its behavior when immersed in water. Further, these data show that a sensor's performance in water is not significantly affected by its prior immersion in a dilute polymer solution.

Evaluating the hot-film's performance in a more quantitative manner, the calibration curve of bridge power per °C of overheat vs. wall shear velocity $[E_B^2/(R_F\ \Delta T)$ vs. $U_\tau]$ determined for a specific sensor in pure water is assumed to be valid for the sensor in the dilute polymer solution. That is, it is assumed that the wall shear velocity in polymer can be calculated using the equation

$$U_{\tau,p} = \left[\frac{\left(\frac{E_B^2}{R_F\ \Delta T}\right)_{polymer} - B}{A}\right]^{3/2} \qquad (4.10)$$

where A and B are the calibration constants established for the specific sensor in water. Such would be the case if hot-film sensors possessed the same performance characteristics in both water and dilute polymer solution

Figure 22 shows the wall shear velocity as a function of disk rotation rate for the dilute polymer data of Figures 20 and 21.

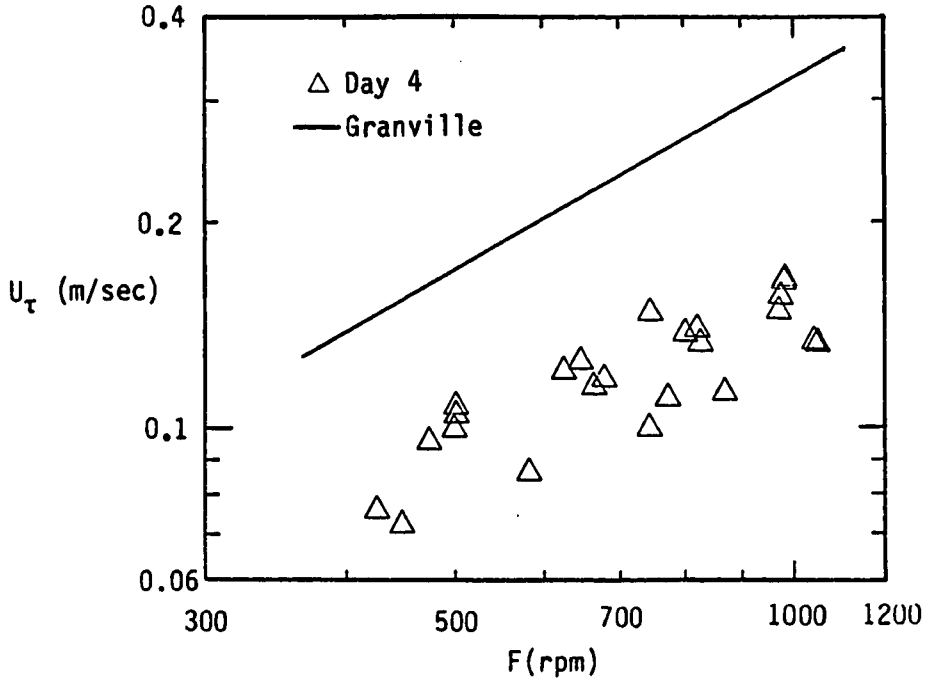

a) Sensor F at (r/R) = 0.57 on Day 4

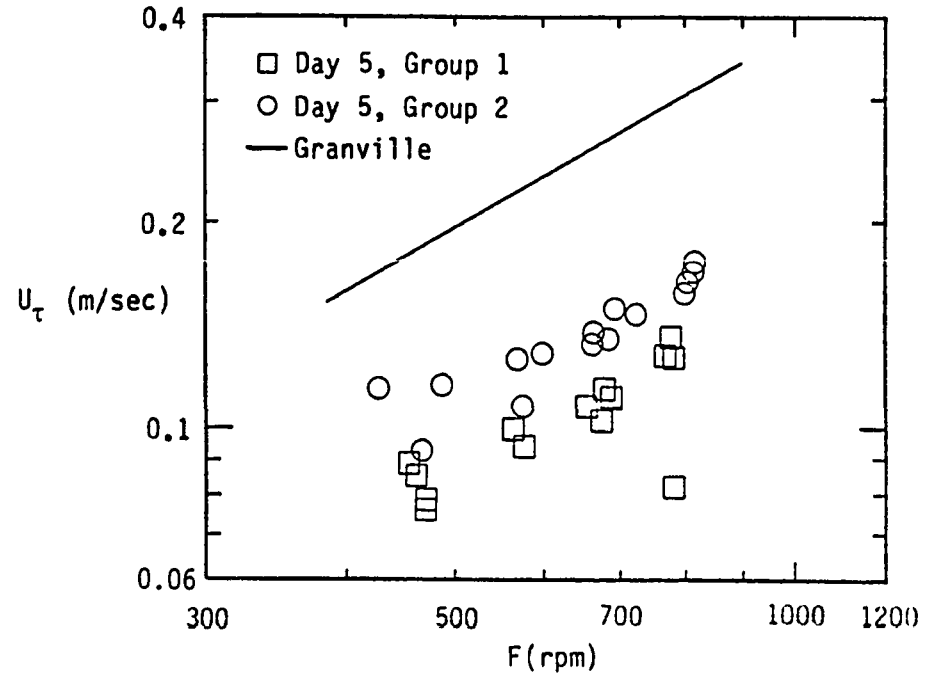

b) Sensor G at (r/R) = 0.68 on Day 5

Figure 22. Wall Shear Velocities as a Function of Disk Rotation Rate, for the Polymer Data Shown in Figures 20 and 21. Granville's Model for Pure Water (1973) is Also Shown

The seemingly larger scatter within each group and the apparent shift between groups in this figure relative to previous measurements is due to the conversion from bridge power to shear velocity [$U_\tau \sim (E_B^2/R_F\Delta T)^{3/2}$]. The scatter for a pure water case would be comparable to that shown for polymer measurements. For comparison, the expected wall shear velocity in water, $U_{\tau,w}$ (equation 4.8), is also shown in Figure 22. The percentage decrease in shear stress due to the polymer is then

$$\% \frac{\Delta\tau}{\tau} = \frac{(U_{\tau,w})^2 - (U_{\tau,p})^2}{(U_{\tau,w})^2} \times 100$$

and this quantity is plotted in Figure 23.

For reference, a least-squares fit to the percentage torque reduction shown in Figure 17 is also shown in Figure 23. It can be seen that the implied skin friction reduction in wall shear stress is 1.5 to 2 times the measured overall torque reduction following the assumption that the hot-film calibrations performed in water are valid in the dilute polymer solution.

From this discrepancy it can be concluded that accurate shear stress measurements in dilute polymer solutions with surface hot-film sensors may not be accomplished with the relatively simple precalibration in water. It appears that the polymer contaminates the sensor so that its heat transfer characteristics are changed and a calibration in the same dilute polymer solution may be required to obtain

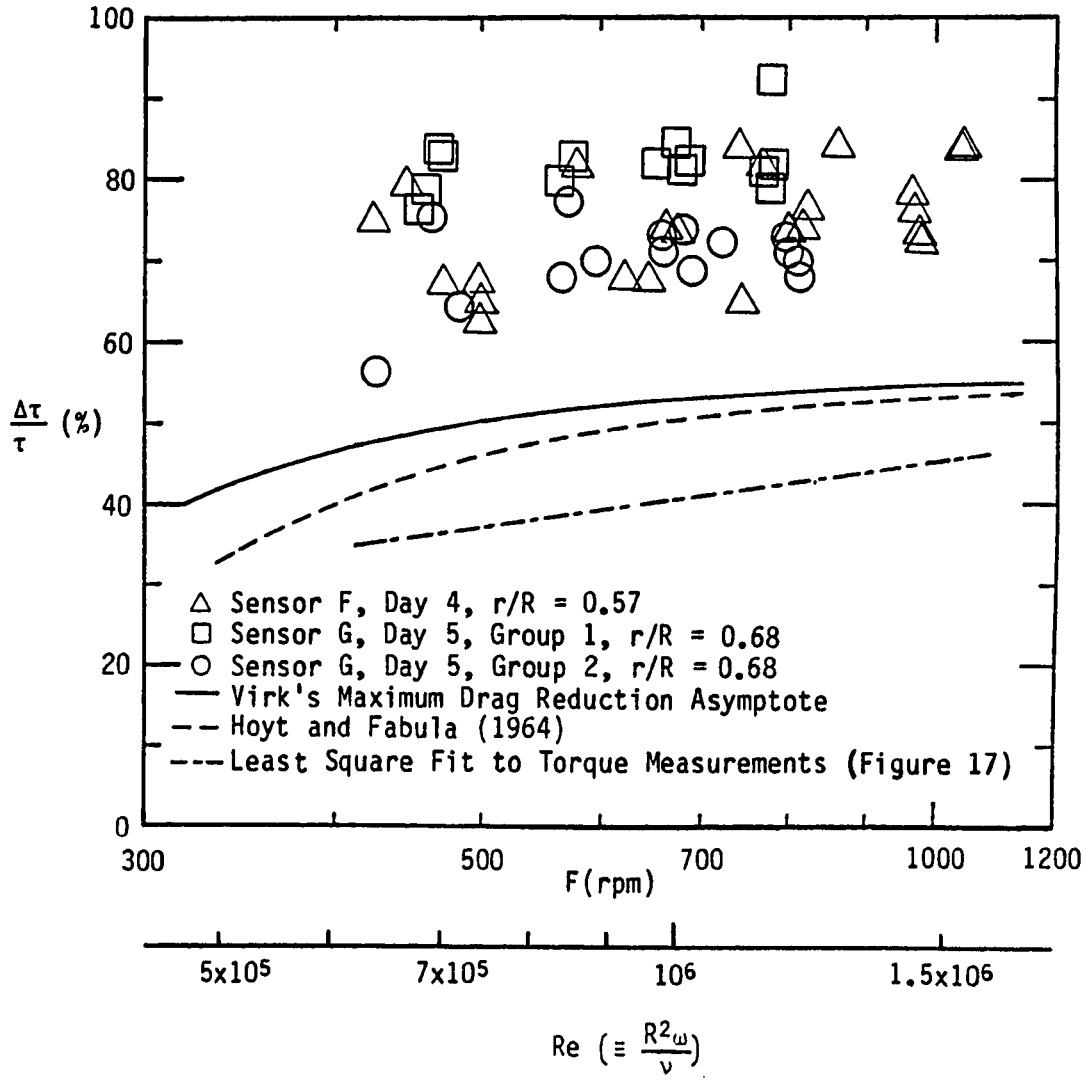

Figure 23. Percentage Reduction in Wall Shear Stress

scientific quality accuracy of measurements. Such was the finding of Lindgren and Chao (1967) in their calibration of hot-film wedge probes in a dilute polymer solution. If the polymer contamination takes the form of a thin coating of concentrated polymer adhering to the hot-film's surface, and if the thickness of such a layer does not change significantly, then a hot-film calibration may be reproducible (if performed in the proper dilute polymer solution). It may also be possible to determine a functional relation between the sensor's calibration in water and in polymer. Either of these possibilities would increase the utility of the hot-film sensors significantly.

4.3 Measurements with Polymer Injection

The polymer injection experiments were designed to produce an immediately measurable effect of the polymer solution on local skin friction measurements. In addition, such an arrangement is a simulation of a practical full-scale system.

Each of these experiments was conducted over a two-minute time frame with 3-second samples taken at intervals of 30 seconds. Two samples were taken prior to injection of polymer, one during injection, and two after.

For the experiments reported here the concentration of the injected solution was 4000 ppm (SEPARAN AP-30) and the injection rate was 25 cc/sec. This particular injection rate was calculated by first estimating the mass flowrate in the boundary layer at the outer edge of the disk. The polymer injection flowrate corresponds to an average

concentration within the boundary layer at the edge of the disk. A lower bound for this average concentration can be estimated from the ratio of (the product of injected flowrate and concentration of the injected solution) and (the pre-injection boundary layer flowrate); this lower bound is denoted in the results. The concentration distribution across the boundary layer has a maximum near the wall and it is the near wall turbulence structure that is most affected by the presence of polymer (Luchik and Tiederman, 1985).

Figure 24 shows two records of 5 sequential measurements of local wall shear stress obtained from hot-film sensors located at r/R = .35 and .57. The data are plotted in terms of apparent percentage skin friction coefficient reduction for convenient comparison with the homogeneous solution data. The skin friction coefficient is given by

$$C_f = \frac{\tau_w}{\frac{1}{2}\rho\omega^2 R^2}$$

Note that the percentage reduction has been normalized to zero at each initial measurement to account for shifts in the hot-film calibration due to previously injected polymer. The indicated skin friction reduction is approximately 65%, which is in good agreement with the experiments conducted in the homogeneous dilute polymer solution presented earlier. Following the injection, the hot-film's output returns to nearly the same level as prior to injection. The return, however, is not complete within the 3-minute experiment, except in the case of the outer probe at F=1000 RPM.

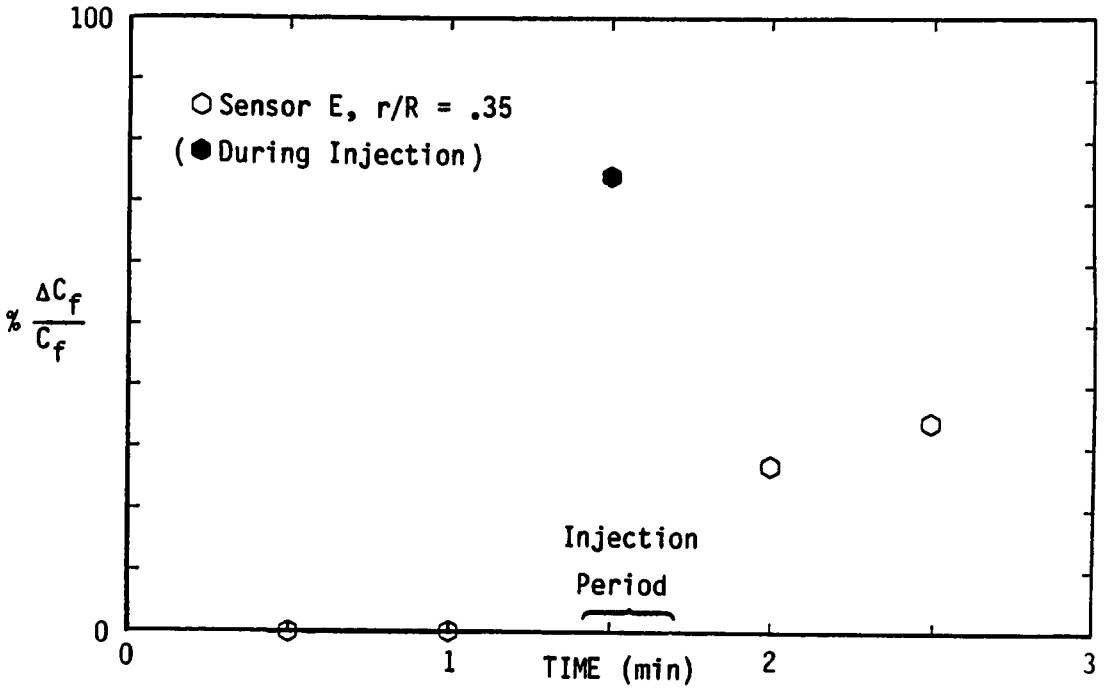

a) Injection at ~800 rpm

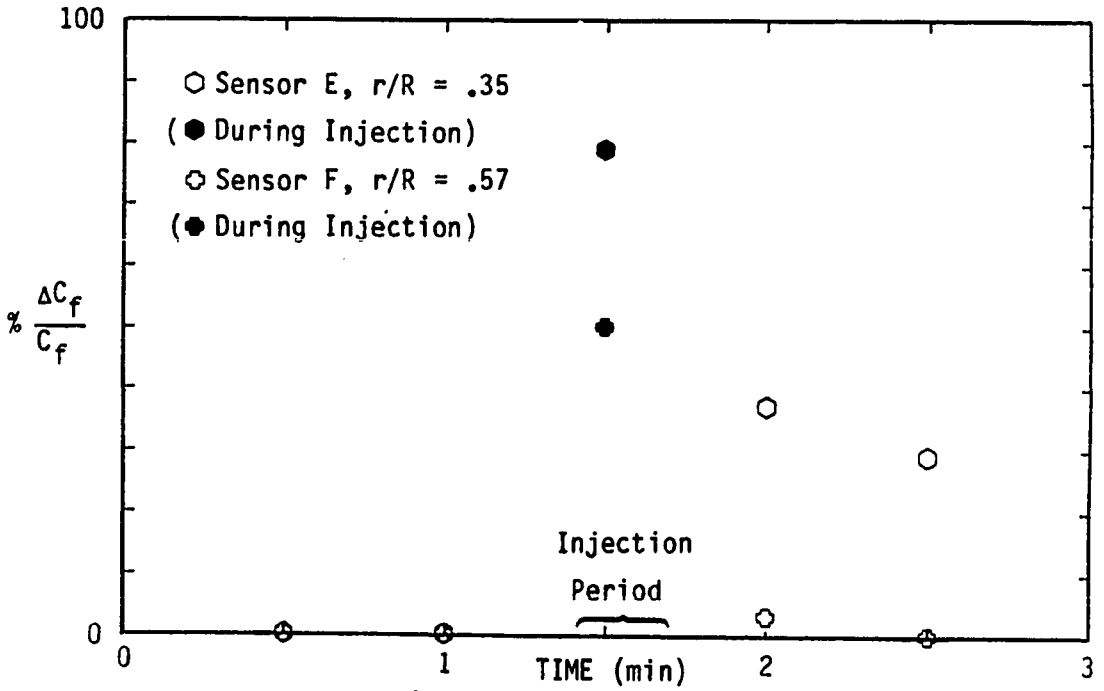

b) Injection at ~1000 rpm

Figure 24. Apparent Skin Friction Coefficient Reduction Measured by Hot-Film Sensors During Two Polymer Injection Experiments

Presumably the shear stress that removes any polymer residue is higher for this outer probe.

For the injection experiments (Figure 24) the input power to the drive motor was held constant. The torque required to drive the disk reduced with polymer injection allowing the disk to increase RPM (Figure 25). For the initial RPM value of 800 (Figure 25a), the increase in RPM is consistent with a 45% drag reduction (on one side of the disk only) that was measured in the homogeneous dilute polymer experiments. The fact that this is not true for the initial RPM of 1000 (Figure 25b) may be attributable to the presence of dilute polymer (13 PPM) in the test tank prior to injection. In the case of injection at F = 1000 rpm (Figure 25b) the disk rotation speed begins to decrease noticeably within 60 seconds after injection. A similar effect cannot be seen in the case of injection at 800 rpm, implying that the viscous polymer may have adhered to the disk and provided drag reduction at the lower rotation rate while being scrubbed from the surface of the disk at the higher rotation rate.

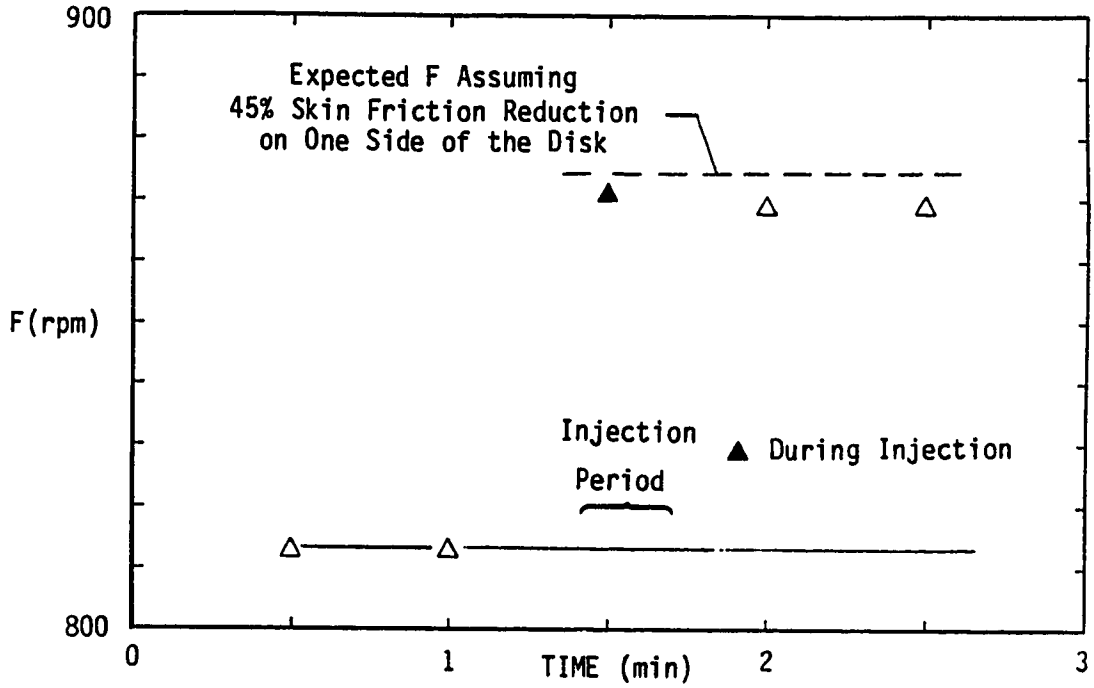

a) Injection at ~800 rpm

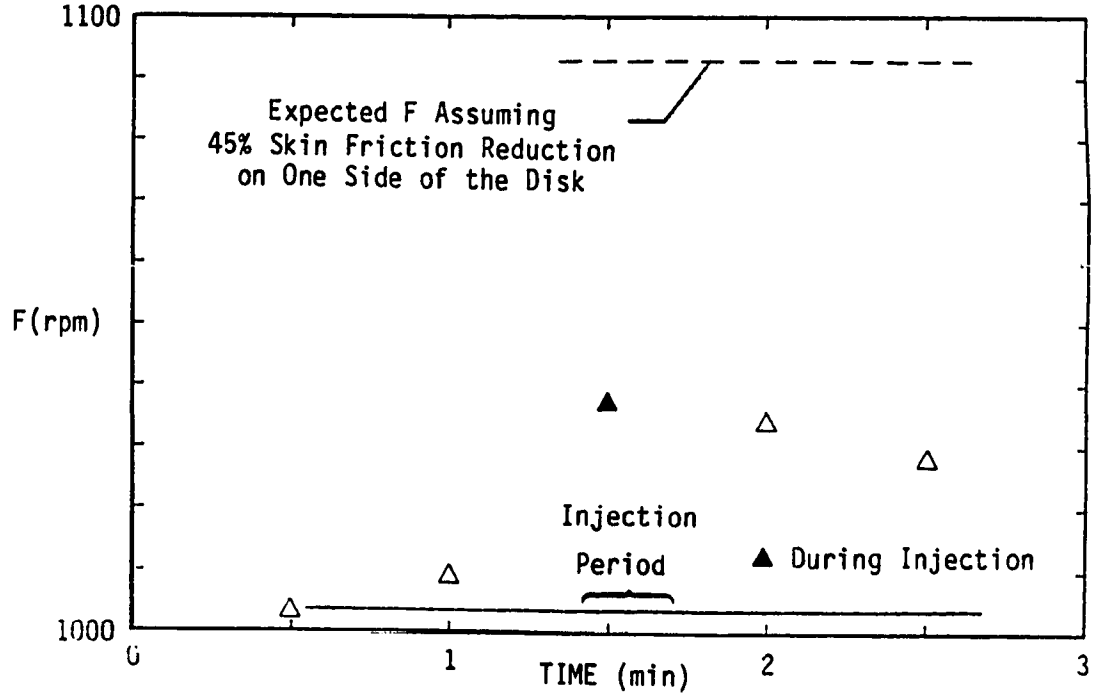

b) Injection at ~1000 rpm

Figure 25. Disk Rotation Rate During Two Polymer Injection Experiments with Constant Motor Input Power

5. CONCLUSIONS

This study has shown that the response of a flush-mounted surface hot-film sensor in a dilute polymer solution is significantly different from its response in pure water. Therefore, accurate skin friction measurements in a dilute polymer flow cannot be obtained by simply using a surface hot-film sensor which has been precalibrated in a pure water flow.

However, it has been seen that the performance of a surface hot-film sensor in a dilute polymer solution apparently does not change with time immersed in the solution. No significant calibration shifts were seen during immersions in polymer of several hours. This implies that reasonably consistent measurements may be obtained with sensors which have been precalibrated in controlled polymer solutions.

Further, it has been observed that a flush-mounted surface hot-film sensor's performance in pure water is not affected by its prior immersion in dilute polymer. That is, a surface hot-film sensor immersed in dilute polymer solution and then placed in pure water will perform in the same manner as it would have if it were immediately immersed in pure water. This fact, combined with the lack of calibration shift of sensors while they are immersed in the polymer solution, imply that the difference in performance of the sensors in pure water and dilute polymer is not due to a continuous "mucus buildup" of long chain polymers on the surface of the flush-mounted sensor. Instead, a thin layer of long chain polymers apparently coats

the surface of the sensor almost immediately and then remains relatively constant in thickness. The fact that the thickness of the polymer coating does not change appreciably in time indicates that it may be possible to determine a functional relationship between the calibration constants of a sensor in water and its calibration constants in dilute polymer solutions. Such a functional relation would allow in situ precalibration of the sensor in pure water immediately prior to its use in dilute polymer.

This study has also shown that drag reduction can be obtained by the injection of concentrated polymer (approximately 4000 ppm) into the boundary layer of a rotating disk in otherwise pure water flow. Drag reduction of the same order as that which can be obtained with dilute polymer solutions can be obtained with this technique. In addition, the performance of the surface hot-film sensors during injection is comparable to their performance in dilute polymer solutions. The consistency of such injection experiments suggests that a new method for testing concentrated polymer solutions has been developed which will allow examination of their dilution and mixing properties, as well as their drag reducing capabilities.

NOMENCLATURE

C_f - Skin Friction Coefficient, $2\tau_w/\rho\omega^2R^2$

C_M - Moment Coefficient of Rotating Disk

$C_{M,K}$ - Theoretical Disk Moment Coefficient in Water from von Kármán (1921)

$C_{M,P}$ - Actual Disk Moment Coefficient in Polymer, Determined from $P_{D,P}$

$E(t)$ - Motor Input Voltage

$\bar{E}$ - Average Motor Input Voltage

E_B - Average Hot-Film Bridge Output Voltage

E_S - Average Voltage Drop Across Hot-Film Sensor

E_L - Average Voltage Drop Across Leads to Hot-Film Sensor

E_R - Average Voltage Drop Across Fixed Resistances in the Hot-Film Bridge

F - Disk Rotation Rate in R.P.M.

$I(t)$ - Motor Input Amperage

$\bar{I}$ - Average Motor Input Amperage

$P_{D,P}$ - Actual Power Delivered to Disk in Polymer

P_I - Motor Input Power

$P_{I,P}$ - Motor Input Power in Polymer

$P_{I,T}$ - Motor Input Power in Air (Tare)

$P_{I,W}$ - Motor Input Power in Water

$P_{K,W}$ - Theoretical Power Required by Disk in Water from von Kármán (1921).

r - Radial Distance

R - Outer Radius of Disk

R_c - Hot-Film Cold Resistance

R_F - Hot-Film Operating Resistance

Pr - Prandtl's Number $(\mu C_p/k)$

Re - Reynold's Number $(\omega R^2/\nu)$

τ_w - Wall Shear Stress

U_τ - Wall Shear Velocity, $\sqrt{\tau_w/\rho}$

$U_{\tau,p}$ - Wall Shear Velocity in Polymer

$U_{\tau,w}$ - Wall Shear Velocity in Water as Determined by Granville (1973)

% DR - Percentage Drag Reduction

$\% \left(\frac{\Delta C_f}{C_f}\right)$ - Percentage Reduction in Skin Friction Coefficient

$\% \frac{\Delta\tau}{\tau}$ - Percentage Reduction in Wall Shear Stress

δ_V - Viscous Sublayer Thickness

δ_T - Turbulent Boundary Layer Thickness

η - Motor Efficiency

ν - Fluid Viscosity

ρ - Fluid Density

ω - Disk Rotation Rate in radians/sec

REFERENCES

Bellhouse, B. J. and Schultz, D. L. (1966) "Determination of Mean and Dynamic Skin Friction Separation and Transition in Low Speed Flow with a Thin Film Heated Element," J. Fluid Mechanics, 24, Part 2, pp. 379-400.

Brown, G. L. and Davey, R. F. (1971) "The Calibration of Hot-Films for Skin Friction Measurement," Rev. of Scientific Instruments, 42, pp. 1729-1731.

Cham, T-S. and Head, M. R. (1969) "Turbulent Boundary-Layer Flow on a Rotating Disk," J. Fluid Mechanics, 37, Part 1, pp. 129-147.

Granville, P. S. (1973) "The Torque and Turbulent Boundary Layer of Rotating Disks with Smooth and Rough Surfaces, and in Drag Reduction Polymer Solutions," J. Ship Research, 17, pp. 181-195.

Hoyt, J. W. and Fabula, A. G. (1964) "The Effect of Additives on Fluid Friction," 5th Symposium on Naval Hydrodynamics, Office of Naval Research ACR-112, U.S.Gov. Printing Office, Washington, DC.

Kalashnikov, V.N. and Kudin, A.M (1973) "Calibration of Hot-Film Probes in Water and Polymer Solutions," DISA Information No. 14.

Kraynik, A. M. and Schowalter, W. R. (1981) "Slip at the Wall and Extrudate Roughness with Aqueous Solutions of Polyvinyl Alcohol and Sodium Borate," J. of Rheology, 25 (1), pp. 95-114.

Liepmann, H. and Skinner, G. (1954) "Shearing-Stress Measurements by Use of a Heated Element," NACA TN 3268.

Lindgren, E. R. and Chao, J. L. (1967) "Application of the Hot-Film Technique on Flow of High-Polymer Solutions," Physics of Fluids, 10, pp. 667.

Luchick, T. A. and Tiederman, W. G. (1985) "Turbulent Structure in Low Concentration Drag Reducing Channel Flows," paper presented at the Drag Reduction and Boundary Layer Control Symposium, National Academy of Sciences, October.

Madavan, N. K., Deutsch, S. and Merkle, C. L. (1985) "Measurements of Local Skin Friction in a Microbubble-Modified Turbulent Boundary Layer," 156, pp. 237-256.

Schlicting, H. (1979) Boundary Layer Theory, 7th Ed., New York, McGraw-Hill.

Tiederman, W. G., Luchik, T. S. and Bogard, D. G. (1985) "Wall-Layer Structure and Drag Reduction," J. of Fluid Mechanics, 156, pp. 419-437.

Virk, P. S., Mickley, H. S. and Smith, K. A. (1970) "The Ultimate Asymptote and Mean Flow Structures in Toms' Phenomenon," Trans. ASME, J. of Applied Mechanics, 37, Series E, No. 2.

von Kármán, Th., (1946) "On Laminar and Turbulent Friction," NACA TM 1092.